Miner Petrol (2013) 107:739–763
DOI 10.1007/s00710-012-0245-3

SPECIAL ISSUE GONDWANA COLLISION

Field, geochemistry and Sr-Nd isotopes of the Pan-African granitoids from the Tifnoute Valley (Sirwa, Anti-Atlas, Morocco): a post-collisional event in a metacratonic setting

A. Toummite · J. P. Liegeois · D. Gasquet · O. Bruguier · E. H. Beraaouz · M. Ikenne

Received: 1 March 2012 / Accepted: 6 November 2012 / Published online: 11 December 2012

Abstract In the Tifnoute Valley, three plutonic units have been defined: the Askaoun intrusion, the Imourkhssen intrusion and the Ougougane group of small intrusions. They are made of quartz diorite, granodiorite and granite and all contain abundant mafic microgranular enclaves (MME). The Askaoun granodiorite and the Imourkhssen granite have been dated by LA-ICP-MS on zircon at 558±2 Ma and 561±3 Ma, respectively. These granitic intrusions are subcontemporaneous to the widespread volcanic and volcano-detrital rocks from the Ouarzazate Group (580–545 Ma), marking the post-collisional transtensional period in the Anti-Atlas and which evolved towards alkaline and tholeiitic lavas in minor volume at the beginning of the Cambrian anorogenic intraplate extensional period. Geochemically, the Tifnoute Valley granitoids belong to an alkali-calcic series (high-K calc-alkaline) with typical Nb-Ta negative anomalies and no alkaline affinities. Granitoids and enclaves display positive $\varepsilon_{Nd\text{-}560Ma}$ (+0.8 to +3.5) with young Nd-T_{DM} between 800 and 1200 Ma and relatively low $^{87}Sr/^{86}Sr$ initial ratios (Sr_i: 0.7034 and 0.7065). These values indicate a mainly juvenile source corresponding to a Pan-African metasomatized lithospheric mantle partly mixed with an old crustal component from the underlying West African Craton (WAC). Preservation in the Anti-Atlas of pre-Pan-African lithologies (c. 2.03 Ga basement, c. 800 Ma passive margin greenschist-facies sediments, allochthonous 750–700 Ma ophiolitic sequences) indicates that the Anti-Atlas lithosphere has not been thickened and was never an active margin during the Neoproterozoic. After a transpressive period, the late Ediacaran period (580–545 Ma) is marked by movement on near vertical transtensional faults, synchronous with the emplacement of the huge Ouarzazate Group and the Tifnoute Valley granitoids. We propose here a geodynamical model where the Tifnoute Valley granitoids as well as the Ouarzazate Group were generated during the post-collisional metacratonic evolution of the northern boundary of the West African craton. The convergence with the peri-Gondwanan active margin produced brittle fracturing of the cratonic boundary without thickening, allowing rising of magmas. The Tifnoute Valley granitoids display a metasomatized lithospheric mantle source mixed with a minor ancient (2 Ga) continental crust component from the underlying WAC.

Editorial handling: T. Abu-Alam

A. Toummite · E. H. Beraaouz · M. Ikenne
LAGAGE, Faculté des Sciences, B.P. 8106, Agadir, Maroc

A. Toummite
e-mail: atoummite@yahoo.fr

E. H. Beraaouz
e-mail: beraaouz@hotmail.com

M. Ikenne
e-mail: ikenne@univ-ibnzohr.ac.ac.ma

J. P. Liegeois
Isotope Geology, Royal Museum for Central Africa, 3080 Tervuren, Belgium

J. P. Liegeois
e-mail: jean-paul.liegeois@africamuseum.be

D. Gasquet (✉)
EDYTEM, Université de Savoie, CNRS, Campus Scientifique, 73376 Le Bourget du Lac Cedex, France
e-mail: dominique.gasquet@univ-savoie.fr

O. Bruguier
Laboratoire ICP-MS Géosciences Montpellier UMR5243-CNRS, Université Montpellier 2, Place E. Bataillon CC060, 34095 Montpellier cedex 05, France

O. Bruguier
e-mail: bruguier@gm.univ-montp2.fr

Introduction

Our understanding of the Neoproterozoic events in the Anti-Atlas belt has largely increased during the last decade due to new geochemical and geochronological data and geodynamical interpretations (Ennih and Liégeois 2001, 2008; Walsh et al. 2002; Samson et al. 2004; Thomas et al. 2002, 2004; Inglis et al. 2004, 2005; Gasquet et al. 2004, 2005, 2008; D'Lemos et al. 2006). However, despite this progress, the significance of the late Neoproterozoic magmatism is still not completely elucidated within the Pan-African evolution of the Anti-Atlas Belt. This Late Neoproterozoic magmatism is felsic, voluminous, potassic, mainly volcanic with the presence of plutons emplaced close to the surface. It has been traditionally interpreted as subduction-related volcanism (Bajja 1987; Saquaque et al. 1989; Regragui 1997; Zahour et al. 1999). However, this interpretation has been challenged by Ennih and Liégeois (2001) who proposed a post-collisional transpressive, evolving to transtensive, environment for that huge felsic magmatism. Since that time, the origin of this magmatism has been a subject of debate (Soulaimani and Piqué 2004; Oudra et al. 2005; Ikenne et al. 2007; Mortaji et al. 2007; Errami et al. 2009).

The northern lithospheric boundary of the West African craton has been considered to be the South Atlas Fault (Fig. 1; SAF; Ennih and Liégeois 2001; 2008). The Tifnoute Valley region has a peculiar position, being located within a protuberance of the Anti-Atlas within the High Atlas range (Fig. 1), being made of Precambrian rocks from the so-called Ouzellarh Salient and the Sirwa Massif (Choubert 1942, 1952; Michard et al. 2010). Together, the Ouzellarh Salient and the Sirwa Massif separate the Cenozoic Ouarzazate basin to the NE and the Souss basin to the SW, which extends towards the Atlantic Ocean. Since they are both uplifted and in a similar manner, we propose here to extend the notion of salient to the Sirwa area and to call it the Ouzellarh-Sirwa Salient (OSS Figs. 1 and 2). This is also justified by the continuity of the basement from Ouzellarh to Sirwa areas as observed in the studied Tifnoute Valley region (Fig. 3).

Limited to the south by the AAMF, the OSS situated between the NHAF and the SAF (Fig. 1) is covered to the SE by the large Cenozoic Sirwa stratovolcano (Berrahma and Delaloye 1989; Liégeois et al. 2005). The OSS is also the locus of the largest Pan-African granitoids outcrops in the Anti-Atlas, indicating that it was a preferential locus for magmatic intrusions and extrusions, including during the Cenozoic (Sirwa stratovolcano).

This paper combines new whole-rock Sr-Nd isotopic data from volcanic rocks and granites from the Tifnoute Valley, in order to identify the source of the magmas. Then, we present zircon U-Pb ages from these rocks and a modelling of the magmatic evolution of the Tifnoute granites. The discussion focuses on the final stages of the geodynamical evolution of the Ouzellarh-Sirwa Salient as this area is fundamental to the understanding of the northern border of the WAC, including current behaviour.

Geological setting

The Anti-Atlas

The Anti-Atlas and High Atlas mountain ranges are parallel and NE–SW elongated (Fig. 1). They are separated by the South Atlas Fault (SAF), which marks the northern boundary of the West African craton (Ennih and Liégeois 2001, 2008). The High Atlas is a Cenozoic fold-thrust assemblage resulting from the inversion of Triassic–Jurassic transtensional rifts related to the Atlantic opening (Frizon de Lamotte et al. 2000; Arboleya et al. 2004; Laville et al. 2004). In contrast, the Anti-Atlas comprises a Palaeoproterozoic basement (2.2–2.0 Ga) and abundant Neoproterozoic rocks covered by Palaeozoic sediments (Figs. 1 and 2). Four orogenies are recorded in the Anti-Atlas: (1) the Eburnian orogeny (2.2–2.0 Ga) generated amphibolite facies metamorphism and magmatism (Thomas et al. 2002 and references therein); (2) the Pan-African orogeny includes several phases from 750 to 550 Ma with abundant magmatism and affected the Eburnian basement mainly through brittle tectonics and fluid percolations (Ennih and Liégeois 2008); (3) the Variscan orogeny induced a shortening that was accommodated by polyharmonic buckle folding of the Palaeozoic sedimentary cover in a thick-skinned fashion during Late Carboniferous to Early Permian times (Burkhard et al. 2006) and do not include magmatism and (4) the Alpine orogeny, inducing in the Anti-Atlas brittle tectonics, uplift and volcanism.

The Neoproterozoic evolution of the Anti-Atlas can be subdivided into five main stages: (1) a c. 800 Ma old passive margin sequence (Tizi n-Taghatine or Taghdout-Lkest Group), 2 km thick, very well preserved, showing beautiful sedimentary features such as ripple marks or desiccation cracks despite the presence of a greenschist-facies metamorphism (Bouougri and Saquaque 2004); (2) several allochthonous ophiolitic sequences (Bou Azzer/Lkst and Sirwa Groups; Leblanc and Lancelot 1980) of intra-oceanic arc type (Leblanc 1976; Bodinier et al. 1984; Beraaouz et al. 2004; Ikenne et al. 2005; Ahmed et al. 2008) whose various stages are dated between 760 and 700 Ma (Thomas et al. 2002; Samson et al. 2004; D'Lemos et al. 2006; El Hadi et al. 2010). Its obduction towards the WAC occurred probably at c. 660 Ma and is marked by an amphibolite facies metamorphism (Thomas et al. 2002). These ophiolitic sequences are located along the Anti-Atlas Major Fault (AAMF), north of which the Eburnian basement is not outcropping; (3) The Saghro Group, formerly considered as a c. 700 Ma island arc series (Saquaque et al. 1989; Hefferan et al. 2002) but actually made of 6 km thick turbiditic series with some intercalation of rift-type tholeiitic basalts (Fekkak et al. 2003) and deposited during the 630–610 Ma time interval

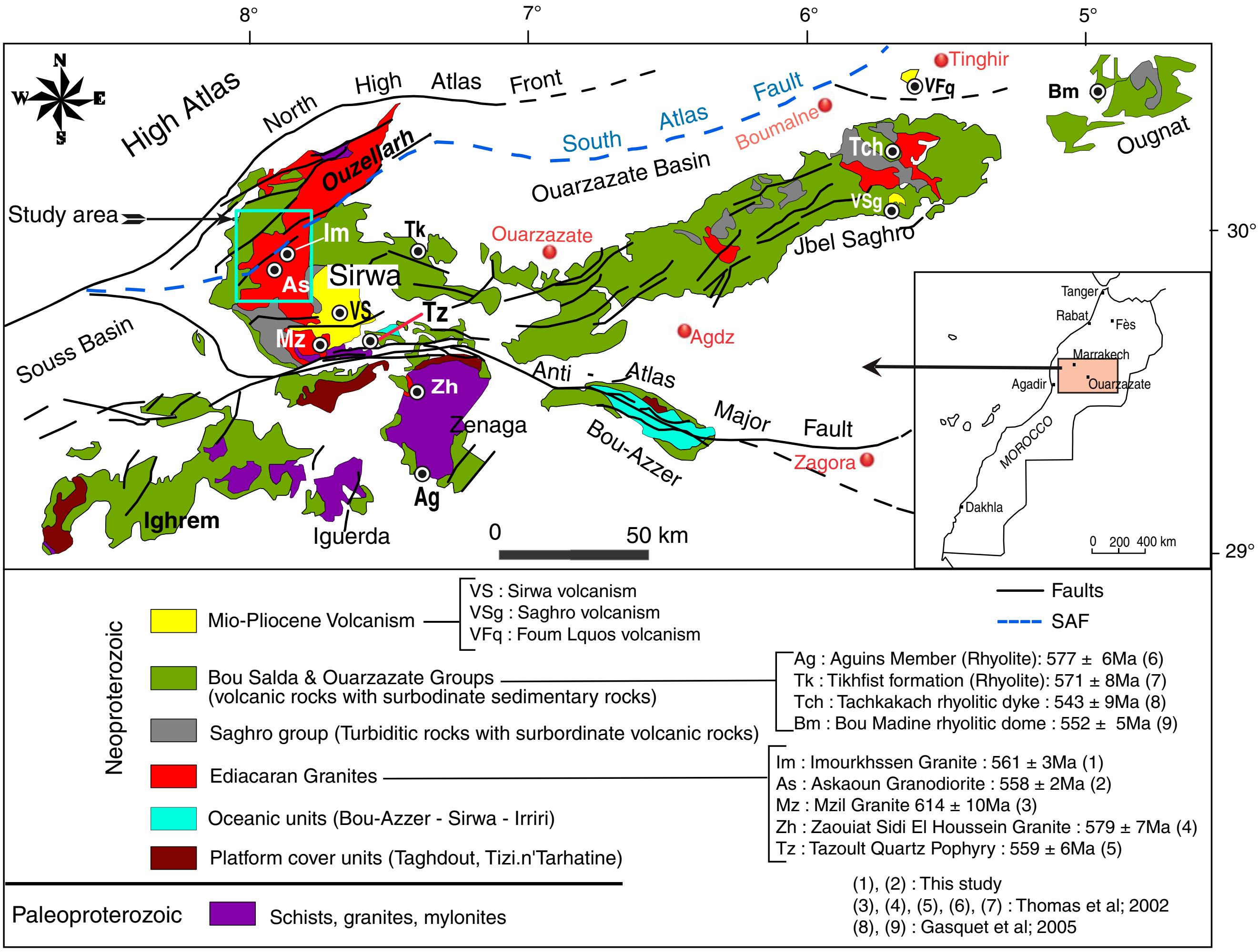

Fig. 1 Schematic map of the Moroccan Anti-Atlas and localization of published Ediacaran magmatic ages. Map modified from Thomas et al. (2002) and Michard et al. (2008)

(Liégeois et al. 2006; Gasquet et al. 2008; Abati et al. 2010); (4) The Bou Salda Group, mostly volcanic and related to a transpressive event (Thomas et al. 2002) emplaced between 610 and 580 Ma (5) The Ouarzazate Group, contemporaneous with the here studied Tifnoute Valley granitoids, covered the whole Anti-Atlas and lasted from 580 to 545 Ma during a transtensional context (Gasquet et al. 2008 and references therein). The Bou Salda Group is actually the precursor of the Ouarzazate Group, which together form the Ouarzazate Supergroup (Thomas et al. 2004). This huge and protracted late Ediacaran magmatic event (610–545 Ma) emplaced during a strong transtensional tectonic regime was linked to an intense hydrothermal activity that generated major Au-Ag-Co-Cu deposits (Gasquet et al. 2008 and references therein). This hydrothermal event induced greenschist facies alteration of the Eburnian basement, including the mobility of rare earth elements (Ennih and Liégeois 2008). Important vertical movements linked to transtension induced a large variability of the thickness of the Ouarzazate Group from 0 to at least 2500 m. The Ouarzazate volcanism belongs to an alkali-calcic series, high-K calc-alkaline to shoshonitic in composition, dominantly effusive, mainly andesitic at the bottom of the sequence and rhyolitic-ignimbritic towards the top of the sequence (Gasquet et al. 2005).

At the very end of the Neoproterozoic, from 545 Ma, and during the Cambrian, the Anti-Atlas was flooded and covered by sediments with rare alkaline volcanism (Soulaimani et al. 2003; Pouclet et al. 2007). This Cambrian event is also known in the High Atlas range (Pouclet et al. 2008).

The Ouzellarh-Sirwa Salient (OSS)

The OSS, as defined above, is a northern Anti-Atlas bulge located across the South Atlas fault. As a consequence, its northern part, the Ouzellarh Salient (Choubert 1942, 1952) is located within the High Atlas Range. The Taghdout Group is mainly present just to the south of the AAMF,

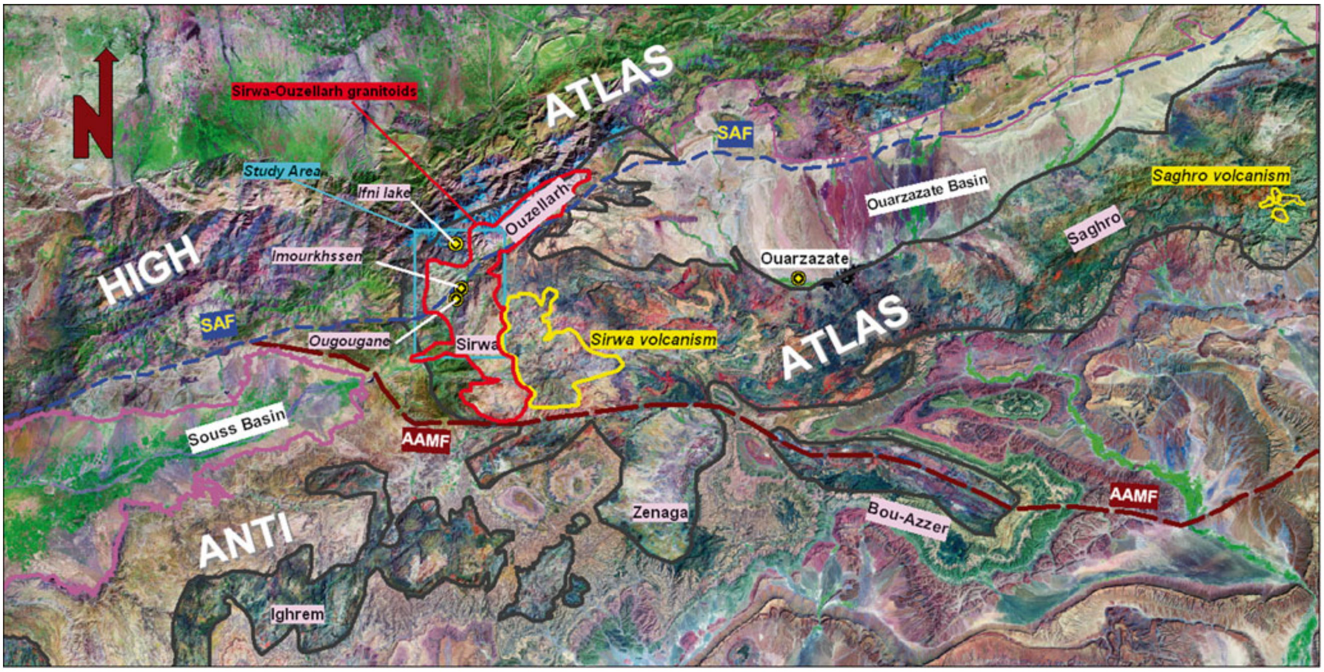

Fig. 2 Satellite photograph of the north–western part of the Anti-Atlas and nearly corresponding to Fig. 1 area. Orthorectified Landsat Thematic Mapper Mosaics as compressed color imagery in MrSID™ file format from Lizardtech. The studied area is outlined in blue. AAMF: Anti-Atlas Major Fault. SAF: South Atlas Fault

above the Eburnian basement of the Zenaga inlier, and represents the Early Neoproterozoic passive margin sedimentary cover (Bouougri and Saquaque 2004). The Bou Azzer-Lkst ophiolitic Group extends along the AAMF and is abundant to the south of the OSS (Thomas et al. 2002). The Saghro Group, mostly present to the south of the SAF, is largely dissected by later tectonic events and its stratigraphy is poorly known in the OSS (Thomas et al. 2002). It is covered by the Bou Salda Group in which rhyolites have been dated at 606±6 and 605±9 Ma close to the Zenaga basement (U-Pb zircon SHRIMP dates; Thomas et al. 2002). Finally the whole assemblage is covered by the huge Ouarzazate Group that extruded between 580 and 545 Ma (Cheilletz et al. 2002; Thomas et al. 2004; Gasquet et al. 2005, 2008). In the field, the Bou Salda (610–580 Ma) and Ouarzazate Groups (580–545 Ma) can be hardly distinguished due to similar textures and clast composition, justifying their assembling in the Ouarzazate Supergroup.

In the OSS, the plutonic rocks are subdivided into three suites: (1) the Assarag suite, comprising two main plutons, Askaoun and Tamtattarn; (2) the Amassine suite, including the Imourkhssen pluton and (3) The Ougougane suite, which includes small late intrusions. All these granitoids comprise abundant mafic microgranular enclaves (MME). They are intrusive within the Ouarzazate volcanoclastic rocks at shallow depth and are crosscut by the important Zaghar mafic dyke swarm, mostly NE–SW oriented. These dykes have generally a meter-size width but can reach 25 m in some cases. Individual dykes can be several km long, the swarm itself being more than 50 km long. The denser part of the Zaghar dyke swarm is located within the Askaoun pluton. The Zaghar dyke swarm, undated, is considered as a late manifestation of the Ouarzazate Group (Thomas et al. 2002).

Petrography of the granitoids and associated rocks

Based on the observation of more than 70 thin sections, we can give the following short petrographical descriptions.

The Assarag magmatic suite

In this study, the Assarag magmatic suite is represented by the Askaoun pluton, which covers a surface of about 600 km^2. In its eastern part, the contact with the hosting volcanodetrital rocks of the Saghro group is sharp. The Askaoun pluton includes quartz diorite and amphibole-biotite granodiorite (Fig. 3). The quartz diorite is grey colored, medium to coarse-grained, with euhedral plagioclase (60–70 % in volume) commonly altered to sericite, quartz (14–17 %), amphibole and biotite. Secondary chlorite, sericite, epidote, and opaque minerals are present. The granodiorite is grey to pink colored and medium-grained; in addition to plagioclase, amphibole and biotite, the quartz crystals form interstitial or poikilitic megacrysts and the K-feldspar (perthitic orthoclase or kaolinitized microcline) appears as anhedral megacrysts. Accessory minerals are apatite, zircon and epidote with rare titanite.

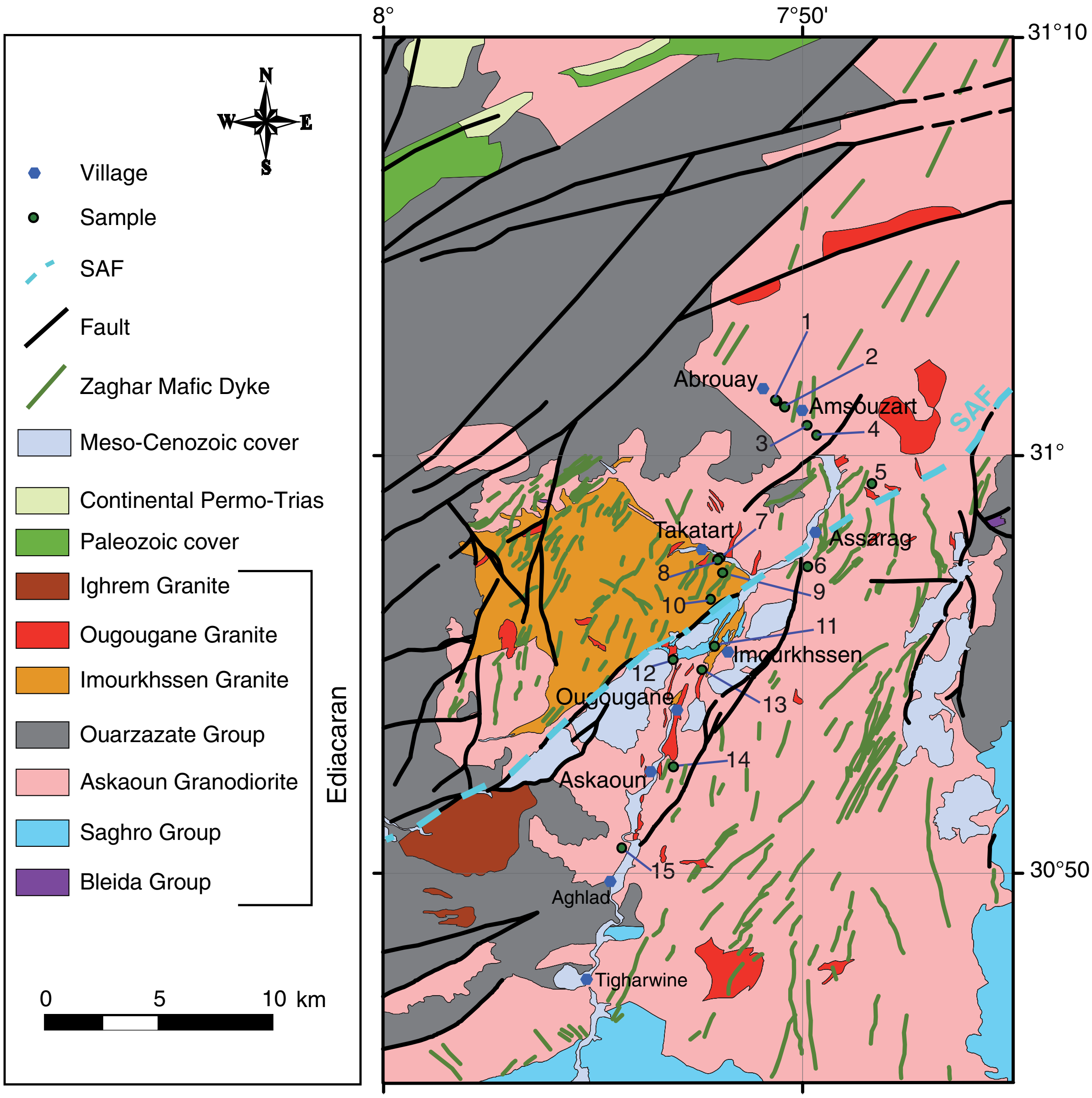

1 : Ab1 (Askaoun granodiorite); Ab1 et Ab6 (microgranular enclave); Ab3 (mafic dyke)
2 : Ab2 (Askaoun granodiorite)
3 : Az1 (Askaoun granodiorite)
4 : Az5 (Askaoun granodiorite); Az2 (mafic dyke)
5 : LT1 (Ougougane Granite)
6 : PTN (Askaoun Granodiorite)
7 : TA4 (Ougougane granite) ; TA6-a ; TA6-b ; TA7 (microgranular enclave).
8 : TA1 et TA2 (Askaoun quartz-Diorite)
9 : AM4 (Imourkhssen Granite)
10 : AM3 (Imourkhssen Granite)
11 : PH10 (Imourkhssen Granite) (U/Pb : 561 ± 3Ma) (This study)
12 : MS7 (Askaoun Granodiorite) (U/Pb : 558 ± 3Ma) (This study)
13 : IM3 ; IM4 (Askaoun Granodiorite) ; IM2 (microgranular enclave)
14 : AS8 (Askaoun Granodiorite)
15 : DZB : Askaoun Granodiorite (U/Pb : 558 ± 2Ma) (This study)

Fig. 3 Geological map of the Tifnoute Valley with the sample location, including those dated. Modified from the geological maps of Thomas et al. (2002) and Choubert (1957)

The Amassine magmatic suite

The main pluton of this suite is the Imourkhssen granitic pluton. It intrudes the volcanodetrital series of the Ouarzazate Group as well as the Askaoun intrusion. This granite is pink colored and coarse-grained and consists of plagioclase (31 %), K-feldspar (30 %), quartz (37 %) and chloritized biotite (<2 %). Accessory minerals include opaque minerals and rare epidote. Texturally, this homogeneous granite is marked by large pink subhedral crystals of K-feldspar and xenomorphic crystals of quartz.

The Ougougane magmatic suite

The small intrusions of this suite intrude the Askaoun and Imourkhssen plutons. They are essentially made of microgranite with the occurrence of some quartz microdiorite in the Takatart area. The quartz microdiorite is a grey colored and fine-grained rock with abundant and large phenocrysts of plagioclase and hornblende (4 mm) in a matrix of quartz and plagioclase. Brown biotite occurs as scattered chloritized phenocrysts. Opaque minerals and epidote occur with hornblende and biotite. The pink colored and fine-grained microgranite (grain size<1 mm) contains abundant interstitial quartz (37 %) and perthitic orthoclase (40 %); the plagioclase occurs as scattered zoned phenocrysts (3 mm in size) and rarely in the matrix. Accessory minerals are biotite, euhedral Fe-Ti oxides and epidote.

Mafic microgranular enclaves (MME)

MME are abundant in the Tifnoute Valley granitoids. They are rounded to ovoid in shape, dark colored and fine grained and generally 5 to 10 cm in size, some reaching a size of 50 cm (Thomas et al. 2004). They are commonly porphyritic and range from microdiorite, quartz microdiorite and micromonzodiorite. The mineral assemblage is similar to those described in their hosting granitoids but with different proportions. Zoned, often altered, plagioclase is preponderant (43–65 %) with abundant hornblende (5–19 %), rarer quartz and subordinate biotite. The monzodiorite contains nearly 20 % of K-feldspar. Ouralitised clinopyroxene has been indentified sporadically from the Abrouay region, for example in sample (Ab6). Accessory minerals include epidote, apatite and euhedral Fe-Ti oxides.

Mafic dykes

The Zaghar mafic dyke swarm is microdioritic, with a slightly porphyritic microlitic groundmass composed of plagioclase with rare Fe-Mg minerals transformed to epidote.

LA-ICP-MS U-Pb zircon dating

Analytical techniques

The sample selected for laser ablation U-Th-Pb geochronology was processed by crushing, heavy liquid and magnetic separation following conventional techniques. Zircons from the non magnetic fractions were hand-picked and mounted along with chips of the G91500 zircon standard (Wiedenbeck et al. 1995) onto adhesive tape. The grains were then enclosed in epoxy resin and polished to expose internal structures. Laser ablation analyses were conducted using a Geolas platform housing a 193 nm CompEx 102 laser from LambdaPhysik, which was connected to an Element XR ICP-MS from ThermoFinnigan at "Laboratoire ICP-MS Géosciences UMR5243-CNRS Montpellier (France)". Details of the analytical procedure are described in Neves et al. (2006) and Dhuime et al. (2007) and are only briefly summarized below. Data were acquired in the peak-jumping mode with the laser operating at an energy density of 15 Jcm^{-2} and a frequency of 3 Hz. The laser spot size was 26 μm. Measured isotopic ratios were monitored with reference to the G91500 zircon standard. Pb/Pb ratios in the unknown zircons were mass-bias corrected using a power law whose parameters were determined by repetitive analysis of the reference material measured during the whole analytical session. This mass bias factor was used to correct the $^{207}Pb/^{206}Pb$ ratios measured on the unknown zircons and its associated error was added in quadrature to the $^{207}Pb/^{206}Pb$ ratios measured on each unknowns following the procedure described in Horstwood et al. (2003). Inter-element fractionation for U and Pb is more sensitive to analytical conditions and the Pb/U ratios of each batch of five unknowns were calibrated against the bias factor calculated using four standards bracketing the five unknowns. The mean Pb/U ratio of the four measured standards was used to calculate the inter-element fractionation and its error was then added in quadrature to the individual error measured on each $^{206}Pb/^{238}U$ unknown. Reproducibility of the standard Pb/U ratio was 0.9 % (RSD; n=24) for the whole LA-ICP-MS session required to analyse the samples and mass bias was 0.21 %. Accurate common lead correction is difficult to achieve, mainly because of the isobaric interference of ^{204}Hg on ^{204}Pb. The contribution of ^{204}Hg on ^{204}Pb was estimated by measuring the ^{202}Hg and assuming a $^{204}Hg/^{202}Hg$ natural isotopic composition of 0.2298. This allows monitoring the common lead content of the analysed grain, but corrections often result in spurious ages. Analyses yielding ^{204}Pb were thus rejected and Table 1 reports only analyses for which no ^{204}Pb was detected. Quoted ratios correspond to measured ratios corrected from background and mass discrimination (+ elemental fractionation for the $^{206}Pb/^{238}U$ ratios). All ages have been calculated using the U and Th decay constants recommended by Steiger and Jäeger (1977). Analytical data were plotted and ages calculated using the IsoplotEx program (Ludwig 2000). Individual analyses in the data Table 1 and in concordia plots are $\pm 1\sigma$ errors and uncertainties in ages are quoted in the text at the 2σ level.

Results

Two samples from the Askaoun granodiorite have been dated. Both samples contain euhedral to subhedral zircon grains which range in color from light yellow to translucent. Sixteen analyses have been performed on twelve zircon grains from sample DZB. All analyses are concordant at about 560 Ma (Fig. 4a) and provide a concordant age of 558 ±2 Ma. Sample MS7 (Fig. 4b) includes (1) a tight concordant group of ten analyses yielding a concordant age of 558 ±3 Ma, (2) inherited cores overgrown by magmatic zircon (as demonstrated by analyses #6-1 and #6-2) yield an age of 588±6 Ma which reflects assimilation of crustal material at depth, probably in the source region of the magma. Both samples provide identical ages of 558 Ma which are interpreted as dating emplacement and crystallisation of the Askaoun granodiorite.

One sample from the Imourkhssen granite (PH10) has also been analysed. Zircon grains are euhedral to subhedral and translucent. Eleven analyses have been performed on nine grains. The analysed grains do not show any age variation and are all tightly concordant at 561 ±3 Ma (Fig. 4c). Zircon morphology suggests an igneous origin, and there is no evidence from the results that the zircon population contains older inherited grains. Therefore, the 561 Ma age is interpreted as the age of zircon crystallisation and emplacement of the granite. This age is identical within error to the age of the Askaoun granodiorite.

Interpretation

The two ages of 558±3 Ma and 558±2 Ma obtained for the Askaoun granodiorite are younger than the age of 575±8 Ma obtained by Thomas et al. (2002). Considering the spread of individual spots along the Concordia obtained by Thomas et al. (2002) and the existence of inherited zircons at 588±6 Ma in sample MS7, it is likely that the older age of Thomas et al. (2002) was influenced by a component of inherited Pb. We thus consider that the Askaoun granodiorite intruded at 558±2 Ma.

The age of 561±3 Ma obtained on the Imourkhssen granite is identical within errors with the age of 562±5 Ma given by Thomas et al. (2002) for the same granite. This age implies that the Askaoun and the Imourkhssen plutons intruded in a short period of time, within a few millions years.

These ages at c. 560 Ma are similar to that of the syn-Ouarzazate Tazoult quartz porphyry (559±6 Ma; Thomas et al. 2002; Fig. 2). Rhyolites from the Ouarzazate Group have been dated at 577±6 Ma (Aguins Member, close to Zenaga basement; Thomas et al., 2002; Fig. 1), 571±8 Ma (Tikhfist Formation, east of OSS; Thomas et al. 2002; Fig. 1), 552±5 Ma (Bou Madine – Ougnat dome, Eastern Saghro; Gasquet et al. 2005) and 543±9 Ma (Tachkakacht dome, Saghro; Gasquet et al. 2005). The obtained ages at c. 560 Ma are thus coeval with the Ouarzazate magmatic activity period and suggest that the studied plutons are subvolcanic manifestions of the volcanic Ouarzazate Group. Slightly older inherited zircons can be related to the Bou Salda Group, the older part of the Ouarzazate Supergroup.

Geochemical characteristics of Tifnoute granitoids and associated rocks

Twenty-two representative samples of different granitoid units, associated MME and mafic dykes have been analysed for major and trace elements (Table 2).

The main magmatic body in the studied region is the Askaoun granodiorite (Fig. 3). It varies from 62 % to 67 % for SiO_2, and from 14.1 % to 15.5 % for Al_2O_3. This granodiorite is peraluminous (A/CNK or ASI: 0.87–1.29), extends on the boundary limiting the calc-alkalic and the alkali-calcic series (Fig. 5a) and belongs to the high-K calc-alkaline series (Fig. 5b). Sample (AZ5) has been strongly albitized (high Na_2O=6.31 %, low K_2O=0.25 % and CaO=1.10 %). Sample (IM4) is albitized to a milder extent, although it yields a very low CaO content (0.59 %). Both samples have also low Sr content (109 and 128 ppm while other granodiorites around 65 % silica have concentrations above 250 ppm). Using the sliding normalization (Liégeois et al. 1998), trace elements confirm that the Askaoun granodiorite belongs to a potassic series and is not alkaline (Fig. 5c), including IM4 and AZ5. Sample AZ5 has a lower mean $[Rb\text{-}Th\text{-}U\text{-}Ta]_{NYTS}$, which is due to a very low content in Rb (5 ppm against around 100 ppm for the other granodiorites) associated with low K and Ba contents as a consequence of albitization (Table 3; Fig 6b). REE patterns (Fig. 6a) are parallel and typical of alkali-calcic series. Samples IM4 and AZ5 are moderately enriched in LREE (La_N: 64–115) and fractionated (La_N/Lu_N: 7–10) with rather flat HREE (Dy_N/Lu_N: 1.04–1.16) and moderate Eu negative anomalies (0.50–0.68). The sum of all REE (ΣREE) ranges from 108 to 178 ppm. Spidergram (Fig. 6b) are also alkali-calcic in character with enrichment in LILE (Large Ion Lithophile Element, K to Th), depletion in Sr and P, resulting from the fractionation of plagioclase and apatite respectively, and Nb-Ta negative anomaly. As

Table 1 LA-ICP-MS U–Pb zircon analyses for Askaoun granodiorite (samples DZB and MS7) and Imourkhssen granite (sample PH10). (Tifnoute Valley)

Analysis	U (ppm)	Th (ppm)	Pb*	Th/Pb	$^{208}Pb/^{206}Pb$	$^{207}Pb/^{206}Pb$	(1σ)	$^{207}Pb/^{235}U$	(1σ)	$^{206}Pb/^{238}U$	(1σ)	Rho	$^{206}Pb/^{238}U$ (±1σ)	$^{207}Pb/^{206}Pb$ (±1σ)	% Conc.
Sample DZB															
#4-1	287	78	26	0.27	0.081	0.0589	0.0007	0.7265	0.0104	0.0895	0.0006	0.49	552.6±3.7	562.5±26.9	98.2
#6-1	308	97	28	0.31	0.093	0.0592	0.0007	0.7312	0.0108	0.0895	0.0007	0.54	552.8±4.2	575.6±26.8	96.0
#10-1	473	131	42	0.28	0.087	0.0588	0.0005	0.7270	0.0100	0.0896	0.0010	0.81	553.3±5.9	560.9±17.5	98.7
#2-2	291	59	25	0.20	0.063	0.0589	0.0005	0.7283	0.0094	0.0897	0.0008	0.70	554.0±4.8	561.9±19.9	98.6
#8-1	287	70	25	0.24	0.074	0.0585	0.0007	0.7235	0.0107	0.0898	0.0008	0.61	554.1±4.8	547.3±25.2	101.2
#2-1	278	75	25	0.27	0.085	0.0594	0.0005	0.7367	0.0109	0.0900	0.0011	0.79	555.3±6.3	581.5±19.4	95.5
#3-2	223	57	20	0.26	0.079	0.0595	0.0006	0.7382	0.0082	0.0900	0.0005	0.47	555.6±2.8	584.7±21.1	95.0
#11-1	618	212	56	0.34	0.119	0.0598	0.0005	0.7427	0.0101	0.0901	0.0010	0.81	556.2±5.8	595.4±17.3	93.4
#3-1	250	65	22	0.26	0.080	0.0589	0.0005	0.7319	0.0093	0.0902	0.0008	0.72	556.7±4.9	561.7±19.0	99.1
#1-2	248	72	23	0.29	0.101	0.0596	0.0006	0.7421	0.0086	0.0903	0.0005	0.51	557.2±3.2	589.8±21.4	94.5
#12-1	443	120	41	0.27	0.117	0.0589	0.0005	0.7348	0.0094	0.0905	0.0008	0.68	558.3±4.7	563.7±20.2	99.0
#5-1	334	121	31	0.36	0.112	0.0592	0.0007	0.7394	0.0110	0.0906	0.0009	0.66	558.8±5.3	575.1±24.2	97.2
#7-1	272	75	25	0.27	0.086	0.0590	0.0008	0.7375	0.0119	0.0907	0.0008	0.55	559.6±4.8	566.6±29.2	98.8
#10-2	484	110	44	0.23	0.071	0.0589	0.0005	0.7436	0.0084	0.0916	0.0008	0.73	565.2±4.5	561.8±16.9	100.6
#1-1	276	80	25	0.29	0.091	0.0593	0.0006	0.7514	0.0112	0.0919	0.0009	0.69	566.5±5.5	579.1±23.3	97.8
#9-1	603	206	56	0.34	0.102	0.0595	0.0006	0.7542	0.0108	0.0919	0.0010	0.75	566.6±5.8	587.0±20.2	96.5
Sample PH10															
#1-1	174	24	15	0.14	0.041	0.0584	0.0007	0.7347	0.0118	0.0912	0.0010	0.68	562.6±5.9	546.0±25.4	103.0
#1-2	168	23	15	0.14	0.044	0.0597	0.0007	0.7458	0.0115	0.0907	0.0009	0.64	559.5±5.3	591.2±25.6	94.6
#2-1	643	168	58	0.26	0.082	0.0590	0.0005	0.7397	0.0112	0.0909	0.0011	0.82	561.1±6.7	566.8±18.9	99.0
#3-1	171	59	16	0.35	0.106	0.0594	0.0006	0.7349	0.0088	0.0897	0.0007	0.61	553.9±3.9	581.8±20.4	95.2
#3-2	192	74	18	0.39	0.122	0.0589	0.0005	0.7276	0.0090	0.0897	0.0008	0.69	553.5±4.5	562.0±19.3	98.5
#4-1	487	118	45	0.24	0.077	0.0589	0.0005	0.7411	0.0087	0.0912	0.0008	0.71	562.7±4.5	564.6±18.1	99.7
#5-1	423	133	39	0.31	0.098	0.0591	0.0005	0.7430	0.0132	0.0912	0.0015	0.89	562.5±8.6	570.9±17.2	98.5
#6-1	590	212	55	0.36	0.109	0.0589	0.0004	0.7435	0.0107	0.0915	0.0011	0.86	564.5±6.6	564.2±16.1	100.0
#7-1	186	70	17	0.38	0.114	0.0590	0.0007	0.7424	0.0142	0.0912	0.0013	0.77	562.9±7.9	567.6±26.5	99.2
#8-1	586	243	55	0.41	0.125	0.0589	0.0005	0.7455	0.0121	0.0918	0.0013	0.86	566.2±7.6	563.1±17.8	100.6
#9-1	616	113	54	0.18	0.057	0.0587	0.0004	0.7426	0.0076	0.0918	0.0007	0.73	565.9±4.0	555.7±15.3	101.8
Sample MS7															
#12-1	1724	777	160	0.45	0.138	0.0596	0.0008	0.7328	0.0132	0.0892	0.0011	0.69	550.6±6.5	589.5±28.1	93.4
#10-1	1860	916	174	0.49	0.138	0.0582	0.0005	0.7179	0.0088	0.0895	0.0007	0.68	552.5±4.4	536.7±19.5	102.9
#5-1	1209	392	110	0.32	0.095	0.0596	0.0006	0.7366	0.0106	0.0896	0.0010	0.76	553.2±5.8	589.7±20.4	93.8
#11-1	379	101	33	0.27	0.076	0.0576	0.0006	0.7118	0.0093	0.0896	0.0007	0.63	553.2±4.4	514.9±22.2	107.4
#6-2 rim	1759	155	150	0.09	0.045	0.0596	0.0006	0.7397	0.0134	0.0900	0.0013	0.81	555.8±7.8	588.3±22.6	94.5

Table 1 (continued)

Analysis	U (ppm)	Th (ppm)	Pb*	Th/Pb	$^{208}Pb/^{206}Pb$	$^{207}Pb/^{206}Pb$	(1σ)	$^{207}Pb/^{235}U$	(1σ)	$^{206}Pb/^{238}U$	(1σ)	Rho	$^{206}Pb/^{238}U$ (±1σ)	$^{207}Pb/^{206}Pb$ (±1σ)	% Conc.
#4-1	274	58	24	0.21	0.062	0.0583	0.0006	0.7246	0.0105	0.0901	0.0009	0.70	556.3±5.4	541.4±22.6	102.8
#2-1	857	231	77	0.27	0.082	0.0586	0.0005	0.7367	0.0097	0.0912	0.0010	0.81	562.9±5.7	550.9±16.7	102.2
#9-1	253	65	23	0.26	0.073	0.0579	0.0006	0.7293	0.0102	0.0914	0.0008	0.63	563.7±4.8	525.6±23.7	107.2
#8-1	312	73	28	0.23	0.067	0.0578	0.0007	0.7298	0.0107	0.0915	0.0007	0.53	564.5±4.2	523.4±26.9	107.9
#7-1	1978	975	189	0.49	0.149	0.0594	0.0006	0.7526	0.0121	0.0919	0.0011	0.76	566.7±6.7	581.7±22.3	97.4
#1-1	325	79	30	0.24	0.076	0.0593	0.0006	0.7779	0.0101	0.0951	0.0007	0.60	585.7±4.4	578.6±22.3	101.2
#6-1 core	884	308	83	0.35	0.101	0.0595	0.0006	0.7807	0.0112	0.0952	0.0010	0.75	586.1±6.0	584.9±20.5	100.2
#1-2	258	69	24	0.27	0.083	0.0588	0.0006	0.7830	0.0103	0.0965	0.0008	0.66	593.9±5.0	561.3±21.3	105.8
#3-1	1285	429	120	0.33	0.099	0.0611	0.0005	0.8173	0.0132	0.0970	0.0013	0.86	596.6±7.9	644.0±17.8	92.6

$^{206}Pb/^{238}U$ (±1σ) and $^{207}Pb/^{206}Pb$ (±1σ) values are ages in million years

Pb*=radiogenic lead in ppm

% Conc. = % concordance

written above, the albitization of sample AZ5 is well expressed by K, Rb and Ba depletions.

The Askaoun quartz diorite outcrops in a restricted area, close to Imourkhssen granite. It is characterized by a silica content around 60 % and differs from the Askaoun main granodiorite by some geochemical differences. The quartz-diorite also lies close the alkali-calcic – calc-alkalic boundary (Fig. 5a), being high-K calc-alkaline (Fig. 5b) and clearly potassic (Fig. 5c). REE patterns (Fig. 6c) are parallel to the Askaoun granodiorite and are similar to the poorer granodiorites in terms of total REE abundance (ΣREE: 106–116) and in LREE (La_N: 63–68). It is slightly less fractionated (La_N/Lu_N: 6.1–6.3) with similar flat HREE (Dy_N/Lu_N: 1.03–1.12) but with nearly no Eu negative anomaly (Eu/Eu* =0.92–0.94). Spidergram have a similar pattern as for the granodiorite with slightly lower Th, Nb, Ta, Ce, Nd contents and slightly higher Zr and Hf contents (Fig. 6d) although the Nb-Ta negative anomaly is still well marked.

The Ougougane granite (71–74 % SiO_2) lies also across the alkali-calcic/calc-alkalic boundary (Fig. 5a), is high-K calc-alkaline (Fig. 5b) and has a global trace element signature similar to the Askaoun granodiorite, if normal differentiation is taken into account (sliding normalization, Fig. 5c). REE patterns (Fig. 6e) are close to that of the Askaoun granodiorite with similar REE abundance (ΣREE: 115–133), LREE enrichment (La_N: 85–107), slightly more fractionated (La_N/Lu_N: 12.6–14.6) due to lower HREE, which are roughly flat (Dy_N/Lu_N: 0.93–1.08) and a moderate Eu negative anomaly (Eu/Eu*=0.57–0.66). Spidergram (Fig. 6f) have a similar pattern but are characterized by a stronger feldspar (lower Sr and Ba) and apatite (lower P) fractionation and a globally lower HFSE content that can be attributed to accessory mineral fractionation such as zircon (lower Zr Hf, Y, Yb) and titanite (lower Ti).

The Imourkhssen granite (74–77 % SiO_2) corresponds at first view to a differentiated Ougougane granite with significant fractionation of feldspar (lower K_2O, Fig. 5b; lower Sr and Ba, Fig. 6h; more negative Eu anomaly, Eu/Eu*=0.37–0.49; Fig. 6g) as well as of apatite (lower P), titanite (lower Ti) and zircon (lower Zr, Hf, Y, Yb) (Fig. 6h). This impoverishment in LILE is important, leading to a distinct position in the NYTS diagram (Fig. 5c) even if the sliding normalization takes into account the silica content of the rocks. REE patterns are close to that of the Ougougane granite although they display higher total REE (ΣREE: 150–154) and LREE (La_N: 105–117) abundances. The REE patterns are less fractionated (La_N/Lu_N: 7.9–8.8) due to a slightly convex HREE pattern (Dy_N/Lu_N: 0.83–0.85), and the Nb-Ta negative anomaly is less pronounced.

The MME analyzed have all been sampled in the Askaoun granodiorite. They show a large range in silica (54–66 % SiO_2), and are centered on the alkali-calcic series (Fig. 5a). The K_2O content is variable (1.37–3.58 %) and

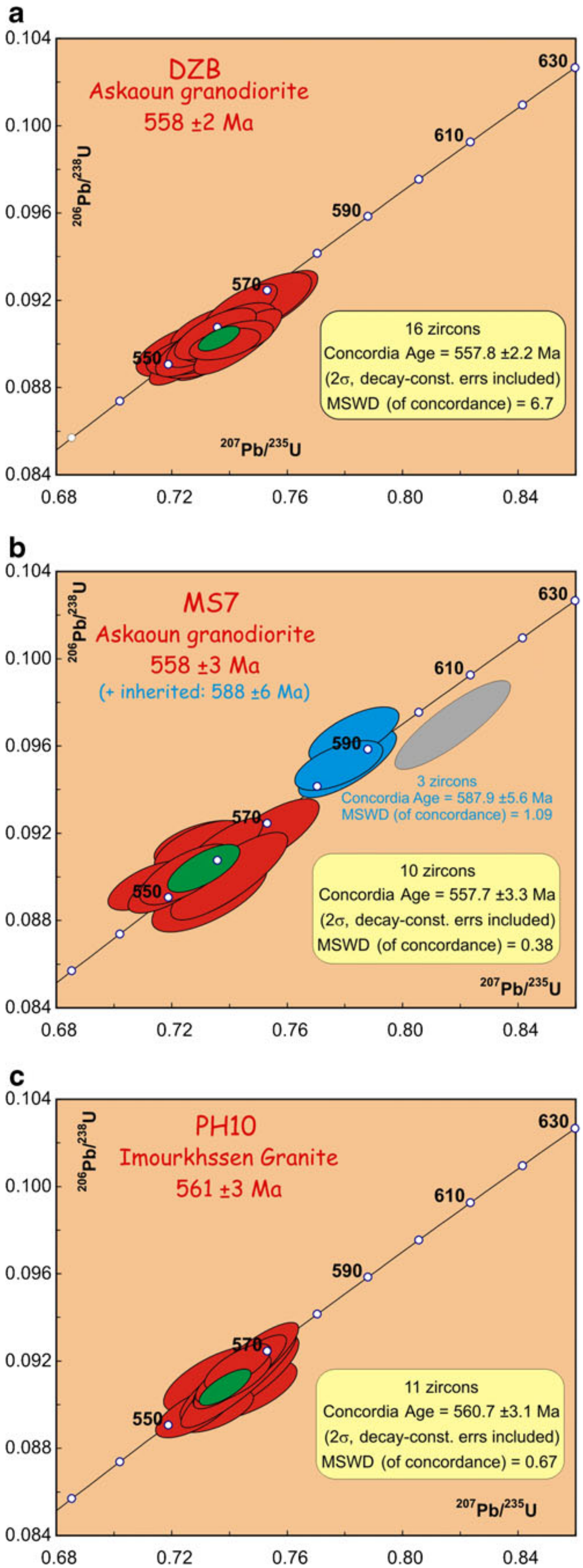

◀**Fig. 4** U-Pb zircon ages. **a** Askaoun granodiorite MS7; **b** Askaoun granodiorite DZB; **c** Imourkhssen granite PH10. Red ellipse=magmatic zircon crystal or rim; blue ellipse=inherited zircon core; grey ellipse=discordant zircon spot not used for age calculation

not correlated with silica (Fig. 5b). This can be related to some alkali mobility, the Na_2O+K_2O being relatively constant (7.4–8.0 %, except the 54 % SiO_2 TA7 sample, 4.7 %), to some possible cumulative character or to interaction with the granodioritic host. Despite this variability, the Askaoun MMEs are all within the potassic field in the NYTS diagram (Fig. 5c). The higher $[Rb\text{-}Th\text{-}U\text{-}Ta]_{NYTS}$ value of sample IM2 is due to a higher U content (8.42 ppm) that can be due to higher mobility of this element in subsurface conditions. The peculiar position of samples Ta6a and Ta6b is due to lower values in Rb and higher values in Y and Yb. This is well seen in their REE patterns (Fig. 6i) that are enriched in LREE, Ta-6b having a seagull pattern suggesting a possible beginning of tetrad effect (enrichment in REE due to F-rich fluids; Bau 1996; Veksler et al. 2005). Sample Ta6a displays a similar enrichment in HREE but is not impoverished in LREE. Such fluid-related disconnection between LREE and HREE behaviour has also been observed in granitoids from the Zenaga Paleoproterozoic basement and has been attributed to complex fluid action generated by the huge Ouarzazate volcanic activity (Ennih and Liégeois 2008). Apart these two samples (TA6a and TA6b), the Askaoun MMEs are moderately but variably enriched in REE (La_N: 42–104), moderately fractionated REE patterns (La_N/Lu_N: 4.5–7.4) with rather flat HREE (Dy_N/Lu_N: 1.12–1.22). Eu is rather constant (13 to 16 times chondrites), implying a deepening of the negative anomaly with REE enrichment (Eu/Eu*: 0.81 to 0.42). Sample TA7, the most basic sample (54 % SiO_2) is the less enriched in REE (ΣREE: 89 ppm), ΣREE ranging in the MME from 89 to 208 ppm, covering the whole span of the studied rocks. Spidergrams (Fig. 6j) display roughly parallel spectra, with enrichment of LILE over HFSE, Nb-Ta negative anomalies, which are attributed to the source, and P and Ti negative anomalies, attributed to magmatic processes. The enrichment in most HFSE and low LILE values displayed by sample Ta6a can be ascribed to their more felsic character (enrichment in incompatible elements) but also to interaction with fluids, as demonstrated by the seagull shape of REE patterns.

The two analyzed Zaghar mafic dykes share some chemical similarities but display also major differences. They are low in silica (48 and 49 % SiO_2), are both in the range of the alkali-calcic series (Fig. 5a) but are medium-K calc-alkaline (Fig. 5b). They are too low in silica to be represented in the NYTS diagram (Liégeois et al. 1998). They show variably enriched REE patterns (Fig. 6k; ΣREE of 94 and 353 ppm) and variable REE fractionation (La_N/Lu_N of 4.9 and 17.5) with however the same content in Lu (0.34 and 0.36 ppm).

Table 2 Major (wt.%) and trace (ppm) element compositions of granitoids and associated rocks for Askaoun, Imourkhssen and Ougougane plutons, including MME and mafic dykes (Tifnoute Valley)

Sample	Askaoun quartz-diorite			Askaoun granodiorite							Imourkhssen granite		Ougougane granite			MME MME					Mafic dykes	
	TA1	TA2	As8	PTN	IM3	IM4	Ab1	Ab2	Az1	Az5	AM3	AM4	LT1	TA4	IM2	TA 6a	TA 7	Ab 1 Encl	Ab6	TA-6b	AB3	Az2
Major elements (wt.%)																						
SiO2	59.25	62.46	61.95	65.52	64.57	65.54	63.94	65.28	63.34	66.99	74.20	76.79	70.76	73.85	57.98	64.07	54.21	57.30	57.79	65.81	48.36	49.00
Al2O3	18.19	16.79	15.52	14.10	15.29	14.81	14.92	14.25	14.91	15.10	12.79	12.70	13.55	13.51	16.17	16.01	14.10	17.10	16.59	15.79	15.09	15.70
Fe2O3t	6.40	4.95	6.68	4.78	5.45	6.04	4.40	4.78	5.92	4.50	1.89	0.76	2.69	1.96	7.97	5.74	9.39	8.20	8.00	5.37	10.16	11.38
MnO	0.13	0.08	0.11	0.04	0.11	0.08	0.07	0.09	0.07	0.05	0.03	0.02	0.05	0.02	0.13	0.08	0.24	0.23	0.15	0.12	0.21	0.20
MgO	2.24	2.24	2.97	1.88	2.89	2.41	1.96	1.99	2.24	3.30	0.45	0.27	0.85	0.69	3.54	1.59	8.98	3.27	3.37	1.77	9.10	10.71
CaO	4.95	2.82	3.87	3.38	2.64	0.59	4.09	2.70	3.04	1.10	0.34	0.12	0.99	1.56	5.31	0.73	6.08	4.13	4.92	2.08	7.76	3.92
Na2O	4.26	4.22	3.60	3.39	3.82	4.20	3.54	3.49	3.65	6.31	3.98	4.90	3.66	3.55	3.78	6.63	2.49	5.88	4.15	5.41	2.69	3.07
K2O	2.14	2.94	3.17	3.66	3.35	3.27	3.64	4.00	3.48	0.25	4.10	3.35	4.54	4.37	3.58	1.37	2.17	1.76	3.23	2.17	0.96	0.33
TiO2	0.58	0.69	0.78	0.59	0.73	0.64	0.67	0.64	0.71	0.67	0.19	0.15	0.34	0.28	0.84	0.62	0.67	1.01	0.89	0.53	1.14	1.00
P2O5	0.17	0.13	0.15	0.10	0.13	0.11	0.12	0.11	0.12	0.13	0.03	0.01	0.04	0.04	0.19	0.25	0.11	0.20	0.17	0.27	0.57	0.19
L.O.I	2.15	2.25	1.81	1.31	1.71	1.87	1.18	1.30	1.38	2.03	0.78	1.28	1.10	0.87	1.18	1.52	2.30	1.44	1.44	1.46	4.83	4.81
Total	100.73	99.58	100.60	98.75	100.69	99.55	98.54	98.63	98.88	100.44	98.77	100.35	98.56	100.70	100.68	98.62	100.74	100.52	100.69	100.79	100.87	100.31
ASI	0.99	1.10	0.95	0.90	1.04	1.29	0.87	0.95	0.97	1.19	1.10	1.07	1.06	1.01	0.82	1.17	0.81	0.90	0.86	1.05	0.77	1.25
Trace elements (ppm)																						
V	91	76	103	73	91	80	79	74	93	66	6	5	31	24	118	29	141	138	120	30	204	186
Rb	88	73	100	139	102	90	80	108	113	5.2	115	81	146	146	121	46	74	55	129	82	18	6.6
Sr	544	368	380	254	230	128	319	273	308	109	82	37	153	175	311	99	285	325	357	280	498	265
Y	19.2	17.0	19.5	19.4	18.0	16.5	20.6	24.8	19.9	13.8	18.5	21.3	10.8	9.9	37.3	52.3	18.7	24.6	19.7	47.9	30.9	19.2
Zr	404	340	257	256	277	245	237	274	234	240	162	130	169	162	208	342	164	202	209	291	186	122
Nb	7.91	7.94	8.65	9.32	11.52	10.33	9.47	9.93	8.94	9.19	12.72	12.81	8.74	7.27	12.03	23.85	5.88	11.39	8.57	19.05	3.88	4.55
Ba	598	817	883	836	907	657	1154	992	840	30.1	605	364	886	706	1010	263	448	358	916	668	1009	185
Hf	9.71	8.46	7.09	7.88	7.69	7.25	7.03	8.20	6.71	6.95	5.39	4.33	5.24	5.18	5.98	8.94	4.47	5.65	5.38	7.45	4.65	3.18
Ta	0.45	0.47	0.58	0.62	0.68	0.84	0.61	0.77	0.62	0.63	1.23	1.13	0.94	0.73	0.78	1.59	0.24	0.77	0.47	1.27	0.12	0.21
W	1.13	0.36	1.91	0.94	1.40	1.37	0.68	0.97	1.05	1.05	0.40	0.89	0.57	0.63	3.36	0.93	0.01	1.86	3.27	0.88	0.71	1.01
Pb	22.75	9.60	24.37	9.23	8.00	18.15	12.12	11.47	13.40	0.82	3.56	0.16	11.42	11.36	12.97	1.89	5.35	14.31	21.56	13.32	7.70	3.07
Th	6.19	8.49	12.41	19.42	14.35	20.12	14.54	17.17	14.81	16.90	15.87	18.52	22.50	25.96	11.72	12.57	4.58	8.50	9.00	9.22	7.86	3.61
U	4.26	4.91	7.16	7.22	7.91	11.61	6.72	8.75	5.44	4.12	6.53	5.21	9.58	8.28	8.42	5.54	2.39	3.16	3.25	3.97	5.97	3.20
La	21.01	19.59	24.7	30.1	23.8	32.9	32.8	35.7	22.7	20.0	34.3	32.5	26.4	33.0	36.57	17.42	13.97	29.07	25.52	33.01	59.80	16.01
Ce	45.73	42.83	53.6	62.6	53.0	73.6	68.3	75.4	51.4	45.9	67.2	65.1	51.4	60.4	84.00	41.51	33.66	64.87	54.21	75.94	145.53	35.61
Pr	5.54	5.09	6.52	7.15	6.35	7.74	7.63	8.97	6.32	5.41	7.42	7.23	5.41	6.18	10.62	5.91	4.36	8.17	6.66	10.06	18.93	4.51
Nd	22.26	19.94	24.62	25.66	24.15	26.66	27.64	33.15	24.03	20.49	25.60	25.45	18.16	20.36	41.39	26.25	17.96	31.55	25.90	41.02	81.94	19.03
Sm	5.09	4.49	5.39	5.10	5.41	5.32	5.62	6.56	5.18	3.89	4.95	4.81	3.62	3.57	9.06	7.27	4.44	6.55	5.65	9.56	16.20	4.13
Eu	1.54	1.32	1.09	0.92	1.14	0.96	1.07	1.03	1.05	0.67	0.75	0.56	0.73	0.63	1.21	0.91	1.12	0.97	1.21	1.12	4.22	1.39

Table 2 (continued)

Sample	Askaoun quartz-diorite		Askaoun granodiorite								Imourkhssen granite		Ougougane granite		MME MME						Mafic dykes	
	TA1	TA2	As8	PTN	IM3	IM4	Ab1	Ab2	Az1	Az5	AM3	AM4	LT1	TA4	IM2	TA 6a	TA 7	Ab 1 Encl	Ab6	TA-6b	AB3	Az2
Gd	4.78	4.12	4.81	4.66	4.52	4.70	4.88	5.75	4.62	3.62	4.28	4.29	3.03	2.98	8.27	7.55	3.89	5.96	5.06	8.93	12.44	4.32
Dy	3.93	3.45	3.88	3.75	3.78	3.68	4.00	4.66	3.87	3.03	3.45	3.57	2.34	2.19	6.86	7.98	3.76	4.74	4.04	8.25	6.59	3.68
Ho	0.83	0.75	0.85	0.80	0.80	0.77	0.85	1.02	0.83	0.67	0.76	0.80	0.49	0.45	1.49	1.81	0.80	1.01	0.82	1.88	1.24	0.83
Er	2.30	2.07	2.26	2.33	2.21	2.19	2.39	2.77	2.27	1.88	2.26	2.38	1.43	1.30	4.05	5.15	2.18	2.82	2.33	5.21	3.00	2.32
Yb	2.30	2.19	2.28	2.27	2.14	2.22	2.36	2.74	2.38	1.90	2.77	2.79	1.48	1.50	3.78	5.49	2.26	2.77	2.28	5.67	2.50	2.21
Lu	0.35	0.33	0.35	0.36	0.33	0.35	0.35	0.40	0.34	0.29	0.41	0.43	0.22	0.23	0.56	0.86	0.32	0.43	0.36	0.86	0.36	0.34
ΣREE	116	106	130	146	128	161	158	178	125	108	154	150	115	133	208	128	89	159	134	202	353	94
Eu/Eu*	0.94	0.92	0.64	0.57	0.68	0.57	0.61	0.50	0.64	0.54	0.49	0.37	0.66	0.57	0.42	0.37	0.81	0.46	0.68	0.36	0.87	1.00
$(La/Lu)_N$	6.25	6.10	7.37	8.80	7.58	9.89	9.73	9.18	6.91	7.13	8.77	7.90	12.63	14.61	6.78	2.10	4.48	7.10	7.44	4.00	17.45	4.90
$(Dy/Lu)_N$	1.12	1.03	1.12	1.05	1.16	1.06	1.14	1.15	1.13	1.04	0.85	0.83	1.08	0.93	1.22	0.93	1.16	1.12	1.13	0.96	1.85	1.08
NYTS - X	0.77	0.72	0.75	0.77	0.72	0.75	0.74	0.89	0.69	0.65	1.05	1.21	0.65	0.71	0.87	1.20	0.49	0.68	0.60	1.23	1.04	0.45
NYTS - Y	1.35	1.09	1.74	1.49	1.58	1.86	1.35	1.56	1.36	0.82	0.94	0.80	1.36	1.20	2.95	1.29	1.41	1.51	1.64	1.05	14.93	2.78

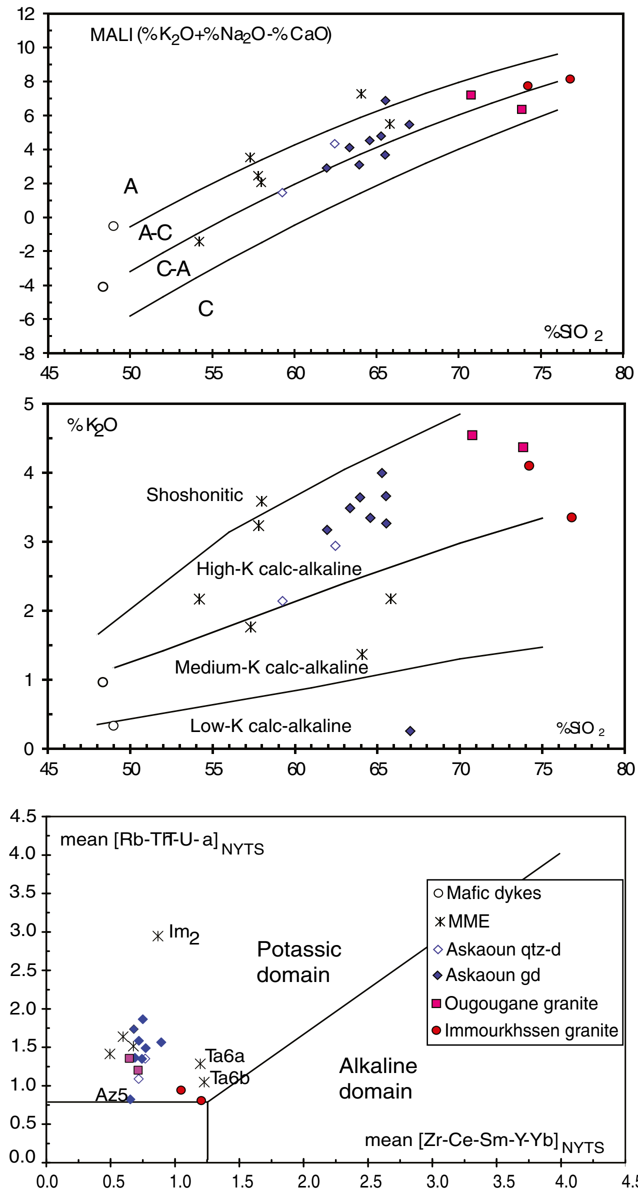

Fig. 5 Tifnoute Valley granitoids and associated rocks in **a** MALI diagram (Modified Alkali-Lime Index; Frost and Frost 2008); **b** SiO_2 vs K_2O diagram with the boundaries between calc-alkaline series of Peccerillo and Taylor 1976; **c** NYTS diagram (sliding normalization to the Yenchichi-Telabit series; Liégeois et al. 1998)

The Eu anomaly is either absent or weak (Eu/Eu*=1 and 0.87). Despite important differences in absolute abundance, the two Zaghar spidergrams (Fig. 6l) appear subparallel with a strong enrichment from Sr to Ba and Th, a major Nb-Ta negative anomaly and a slight decreasing from Ce to Yb. The Sm positive anomaly in sample AB3 relays the LREE enrichment of this sample (Fig. 6k).

Nb-Ta anomaly (calculated as (Nb+Ta)/(Th+Ce), normalized to MORB values) is present in all studied samples but is of variable importance: it varies from 0.4 to 0.5 in the Askaoun granodiorite and quartz diorite, in the Ougougane granite and in most MME. It is lower in the Imourkhssen granite (0.56–0.58), a consequence of its felsic character, and in the two seagull MME (Ta6a and Ta6b, 0.82 and 0.70, respectively). It is higher in the most basic MME (TA7, 0.29) and in the two mafic dykes (0.21 and 0.03), confirming that the Tifnoute Nb-Ta anomaly is a source characteristic.

Sr, Nd isotope composition

Sr and Nd isotopic compositions (Table 2) have been obtained at the Royal Museum for Central Africa on an IsotopX Sector 54 multicollector thermo-ionisation mass spectrometer (TIMS). The average $^{87}Sr/^{86}Sr$ ratio of the NBS SRM987 standard and $^{143}Nd/^{144}Nd$ ratio of the Rennes Nd standard during the period of analyses were 0.710258±10 (2σ on 12 measurements) and 0.511956±9 (2σ on 16 measurements), respectively. Sample ratios have been standardized to a value of 0.710250 for NBS987 and to 0.511963 for the Merck standard (corresponding to a La Jolla value of 0.511858). Data are given in Table 3. The initial ε_{Nd} and $(^{87}Sr/^{86}Sr)_i$ values recalculated at 560 Ma (zircon ages, see above) are shown in Fig 7.

All the studied magmatic rocks have a depleted signature, with positive ε_{Nd} and relatively low $(^{87}Sr/^{86}Sr)_i$, indicating a largely juvenile source, either the mantle or a young lower crust recently formed from the mantle. Indeed the Tifnoute granitoids and associated rocks have $\varepsilon_{Nd\text{-}560\ Ma}$ between +0.8 and+3.5 (up to +5.9 when considering the Zaghar mafic dykes) and $(^{87}Sr/^{86}Sr)_i$, between 0.7034 and 0.7065 (not considering the two Imourkhssen samples with too high Rb/Sr ratios for getting meaningful initial Sr isotopic ratios) (Fig. 7a). These Nd and Sr initial isotopic ratios are similar to that of the Ouarzazate rhyolites from the area (Thomas et al. 2002), confirming a common origin. By opposition, they are more juvenile than those measured eastward in the Saghro region (Fig. 7b; Errami et al. 2009). They are also far from the signature of the nearby Eburnian basement (Zenaga complex; Ennih and Liégeois 2008; Fig. 7c), indicating a minor participation of the latter in the generation of the Tifnoute granitoids. The juvenile character is confirmed by the Nd T_{DM} model ages, which are in the range 800–1200 Ma (down to 650 Ma when considering the Zaghar mafic dykes) (Fig. 7c). There are some variations in these initial isotopic ratios but they are not linked to the silica content of the rocks (Fig. 7d, e). Even if extending from 54 % to 77 % SiO_2, the mean initial Nd and Sr initial ratios are constant. Only the Zaghar mafic dykes show distinctly higher ε_{Nd} (Fig. 7e). The relatively large variations observed in the initial Sr isotopic ratios (Fig. 7d), even in one single pluton, point to some mobility of alkali and alkali-earth elements. This can be attributed to the overlying subcontemporaneous volcanic Ouarzazate Supergroup as demonstrated in the Zenaga basement (Ennih and Liégeois 2008) or to younger events such as the Variscan orogeny, which may be the origin of some ore deposits in the Anti-Atlas (Gasquet et al. 2005).

Modelling of the magmatic evolution of the Tifnoute granitoids

Considering that the Tifnoute granitoids intruded in a short period of time (within age error limits, ±3 m.y.) and have a rather homogeneous mostly juvenile signature, it is wise evaluating if they belong to a single magmatic differentiation or not. For that purpose, we modelled the observed geochemical evolution by using (1) the major elements with a mass balance calculation (Fig. 8; PETROMODE software, Christiansen, pers. comm.) and (2) we calculated the evolution of trace elements using partition coefficients available in the literature and the modal mineral proportion obtained from the major elements (Fig. 9). We compared these calculated results with the measured trace element concentrations of the rocks, thus testing independently the results obtained through the major element mass balance.

The mass balance calculation has been based on trends taking sample TA1 (Askaoun quartz diorite), the most mafic granitoid sample (59 % SiO_2) as parent magma. Isotopes have shown that alkali and alkali-earth elements have been partly mobile. Samples obviously hydrothermally affected have been discarded in this modelling, such as sample AZ5 with 6.3 % Na_2O and 0.25 % K_2O. After this screening, five trends have been calculated towards three Askaoun granodiorites (AS8, AZ1, IM3) for covering the observed variability, one Ougougane granite (LT1) and one Imourkhssen granite (AM3). A sixth trend has been envisaged from Ougougane granite LT1 towards Imourkhssen granite AM3 but no acceptable results have been obtained (residual sum of squares (RSS) >1), indicating that the Imourkhssen granite is not a differentiated product of the Ougougane granite. Calculated trends are represented in Fig 8 and the results are given in Table 4.

The three trends towards the Askaoun granodiorites give similar cumulate compositions and fractional crystallization rates between 57 % and 62 % with low RSS (0.03–0.29). Obtained cumulates are biotite quartz diorites: 66–70 % plagioclase, 9–11 % quartz, 13–14 % biotite, 3–5 % magnetite and 0.2–0.7 % apatite. Some variability occurs in the amphibole/pyroxene content: 0.7 and 6.2 % hornblende for AS8 and AZ1 trends, respectively and 2.9 % clinopyroxene for IM3 trend. The Ougougane granite LT1 (72.6 % SiO_2) is a prolongation of the trend defined by granodiorite AZ1 (65 % SiO_2) with FC rate of 79 % in the case of AZ1, the two cumulates being similar: 63 % plagioclase (66 % for

Table 3 Sm-Nd and Rb-Sr isotopic data of granitoids and associated rock from the Tifnoute Valley

	Rb	Sr	$^{87}Rb/^{86}Sr$	$^{87}Sr/^{86}Sr$	2σ	Sri $_{560\ Ma}$	Sm	Nd	$^{147}Sm/^{144}Nd$	$^{143}Nd/^{144}Nd$	2σ	$\varepsilon_{Nd\ (560\ Ma)}$	T_{DM} (Ma)
Askaoun qz-diorite													
TA1	88.5	544	0.4707	0.708663	0.000010	0.704905	5.09	22.26	0.13844	0.512567	0.000008	+ 2.79	969
TA2	73.4	368	0.5784	0.710019	0.000009	0.705401	4.49	19.94	0.13625	0.512532	0.000008	+ 2.25	1010
Askaoun Granodiorite													
PTN	139	254	1.5840	0.716860	0.000007	0.704214	5.10	25.66	0.12024	0.512459	0.000008	+ 1.98	957
IM3	102	230	1.2816	0.715028	0.000013	0.704796	5.41	24.15	0.13547	0.512592	0.000012	+ 3.49	886
IM4	90.5	128	2.0513	0.719770	0.000010	0.703393	5.32	26.66	0.12081	0.512433	0.000009	+ 1.44	1004
Ab1	80.1	319	0.7262	0.710469	0.000008	0.704671	5.62	27.64	0.12300	0.512475	0.000010	+ 2.10	959
Ab2	108	273	1.1448	0.714680	0.000008	0.705540	6.56	33.15	0.11967	0.512450	0.000010	+ 1.85	966
Az1	113	308	1.0637	0.714135	0.000009	0.705643	5.18	24.03	0.13041	0.512494	0.000010	+ 1.93	1009
Az5	5.2	109	0.1379	0.706086	0.000010	0.704985	3.89	20.49	0.11480	0.512511	0.000011	+ 3.39	828
As8	99.8	380	0.7607	0.711108	0.000009	0.705035	5.39	24.62	0.13231	0.512499	0.000011	+ 1.90	1022
Imourkhssen granite													
AM3	115	82	4.0445	0.734146	0.000010	0.701855	4.95	25.60	0.11693	0.512486	0.000013	+ 2.74	885
AM4	80.8	37	6.3651	0.743954	0.000009	0.693137	4.81	25.45	0.11440	0.512482	0.000009	+ 2.84	869
Ougougane granite													
LT1	146	153	2.7788	0.726105	0.000008	0.703920	3.62	18.16	0.12045	0.512400	0.000007	+ 0.81	1054
TA4	146	175	2.4140	0.724464	0.000010	0.705192	3.57	20.36	0.10618	0.512412	0.000011	+ 2.06	901
MME													
IM2	121	311	1.1246	0.713296	0.000007	0.704318	9.06	41.39	0.13235	0.512499	0.000012	+ 1.90	1022
TA 6a	46.3	99	1.3499	0.714552	0.000016	0.703775	7.27	26.25	0.16756	0.512673	0.000007	+ 2.77	1218
TA 7	74.4	285	0.7566	0.709844	0.000009	0.703803	4.44	17.96	0.14970	0.512594	0.000008	+ 2.51	1071
Ab 1 Encl	54.6	325	0.4865	0.710366	0.000008	0.706482	6.55	31.55	0.12557	0.512462	0.000010	+ 1.66	1008
Ab6	129	357	1.0493	0.714101	0.000008	0.705724	5.65	25.90	0.13197	0.512479	0.000011	+ 1.53	1054
TA-6b	82.2	280	0.8505	0.713040	0.000009	0.706250	9.56	41.02	0.14101	0.512599	0.000010	+ 3.23	937
Mafic dykes													
AB3	18.3	498	0.1065	0.705317	0.000008	0.704467	16.20	81.94	0.11962	0.512656	0.000010	+ 5.87	643
Az2	6.6	265	0.0722	0.705518	0.000011	0.704942	4.13	19.03	0.13117	0.512645	0.000010	+ 4.83	748

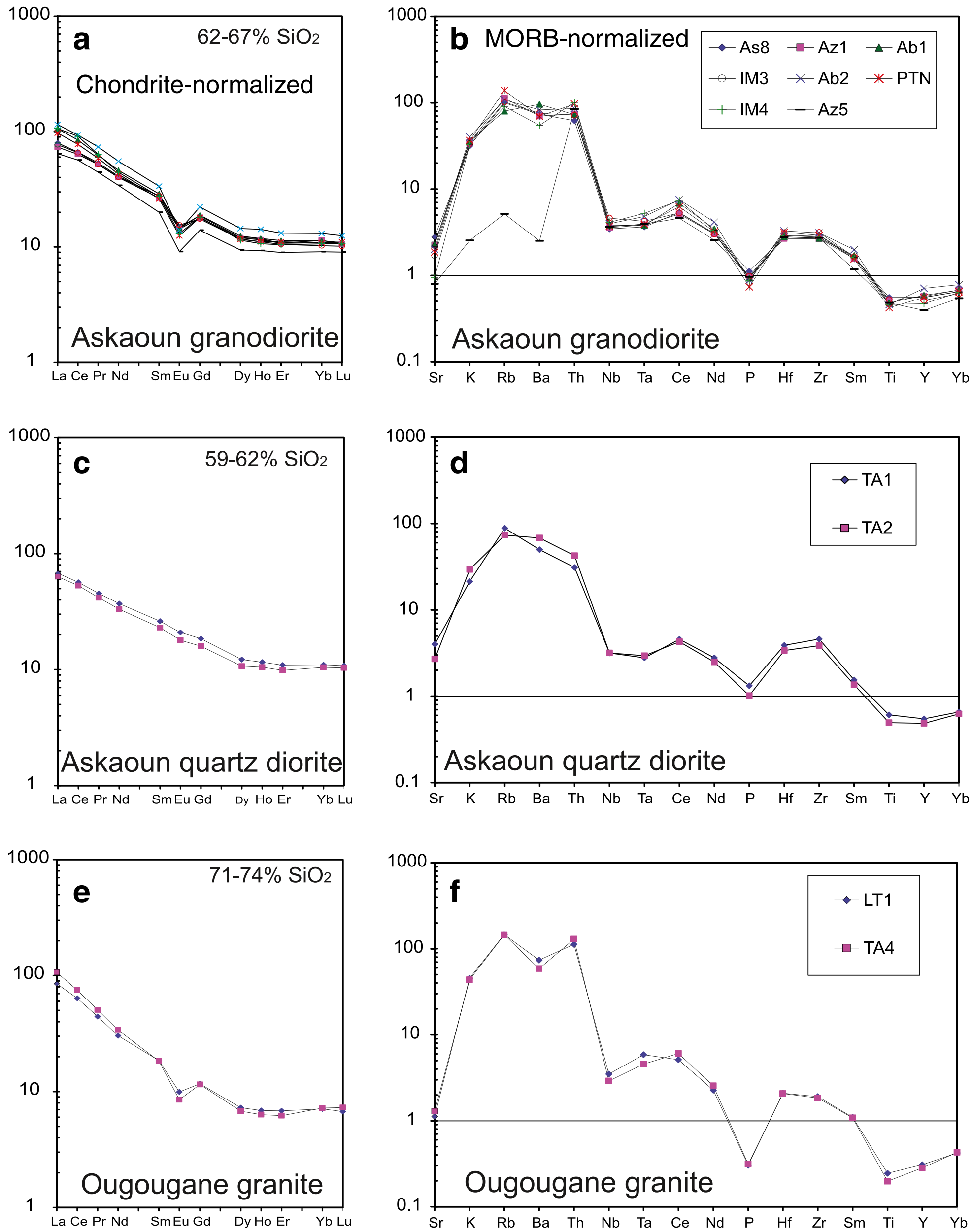

Fig. 6 Chondrite-normalized REE (Evensen et al. 1978) and MORB-normalized (Pearce 1980; Pearce et al. 1984) patterns for the Tifnoute Valley granitoids and associated rocks. **a** and **b**: Askaoun granodiorite; **c** and **d**: Askaoun mafic magmatic enclaves (MME); **e** and **f**: Askaoun quartz diorite; **g** and **h**: Ougougane granite; **i** and **j**: Imourkhsen granite; **k** and **l**: Zaghar mafic dykes

AZ1), 10 % quartz (10 %), 15 % biotite (14 %), 8.6 % hornblende (6.2 %), 2.77 % magnetite (2.75 %), 0.27 % apatite (0.24 %). This is in agreement with the field relationships, showing that the Ougougane granite is a local differentiated product of the Askaoun granodiorite all over the massif (Fig. 3).

The AM3 Imourkhssen granite displays a cumulate with the same minerals but with less quartz and more hornblende (Table 4) indicating slightly different conditions of magmatic differentiation or a slightly different source. Although this pluton is affected by a higher alteration degree (local development of molybdenite flakes; Thomas et al. 2002), we worked on weakly altered samples. We attribute this slight difference in the differentiation to its development as a large pluton (Fig. 3), itself probably linked to the proximity of the South Atlas Fault. The SAF is a current tectonic feature but it also corresponds to the reactivation of a pre-existing major Pan-African lithospheric fault (Ennih and Liégeois 2001, 2008).

Despite a large silica range (60 % to 75 % SiO_2), implying important differentiation rates (between 57 % and 79 %), the REE patterns of studied granitoids are remarkably

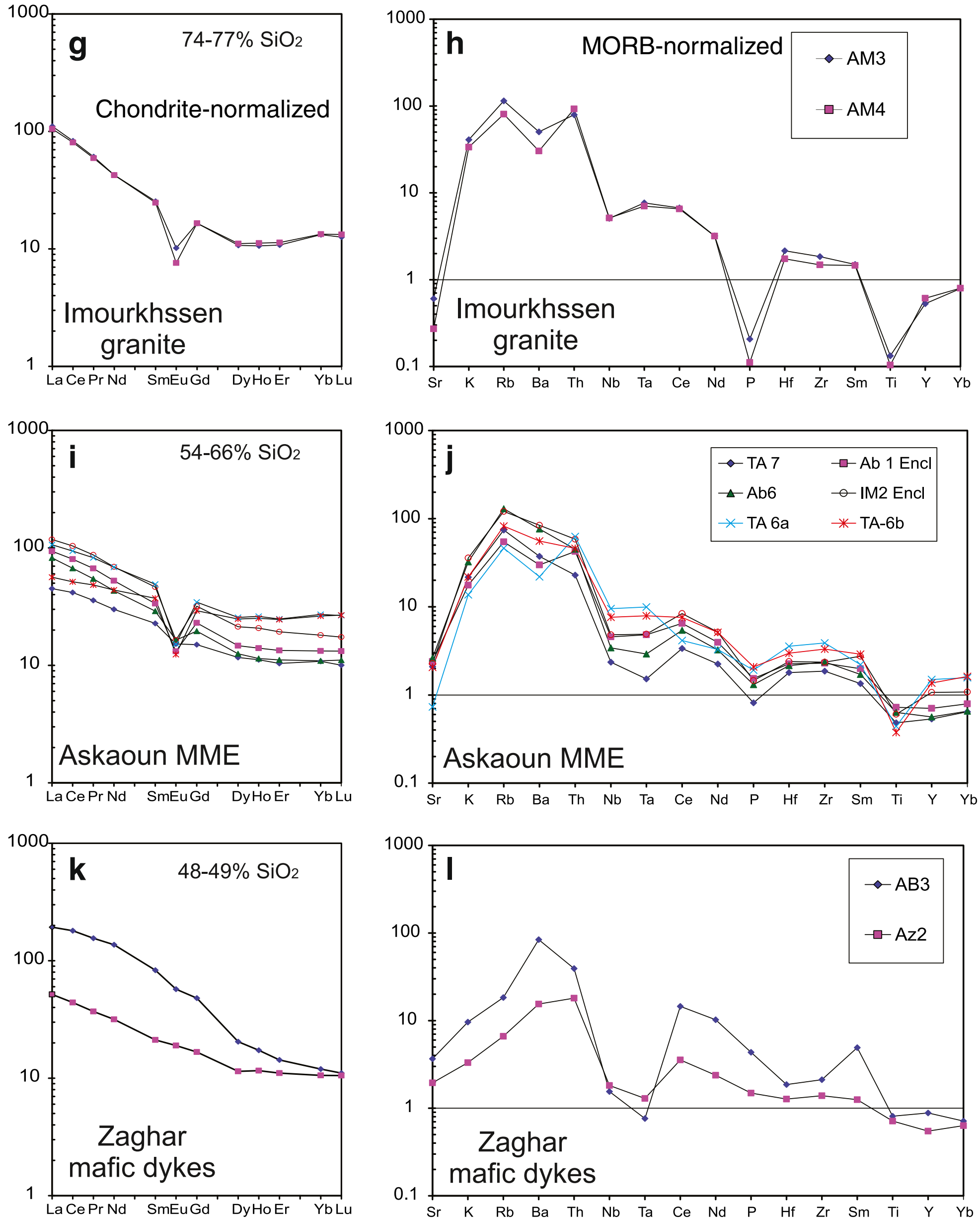

Fig. 6 (continued)

similar in shape and comparable in abundance, from quartz diorite to granites (Fig. 6a, c, e, g). The calculated cumulate compositions are in agreement with this observation (Fig. 9). In this REE modelling, we used the Kd values specified in the figure and the mineral proportions and crystal fractionation rate calculated with the major elements. A few accessory minerals not influencing the major elements but essential for trace elements have been added, i.e. allanite, zircon and titanite. Results are given in Table 4 and shown in Fig. 9. The calculated REE patterns are very close to the measured REE patterns, indicating that the calculated cumulates are in agreement with both major and rare-earth elements. These cumulates have been reported in Fig. 8 together with the Askaoun MME. The large K_2O variability of the MME indicates interactions with the host magma and/or late fluid modifications including albitization (as shown by the very low K_2O content of AZ5; Fig. 8). Considering both major and trace elements, only one MME (AB1) could represent cumulative phases.

Discussion and conclusion

The Tifnoute Valley granitoids are subvolcanic and closely associated with the volcanic Ouarzazate Group. They are here dated at 558±2 Ma and 561±3 Ma, which corresponds

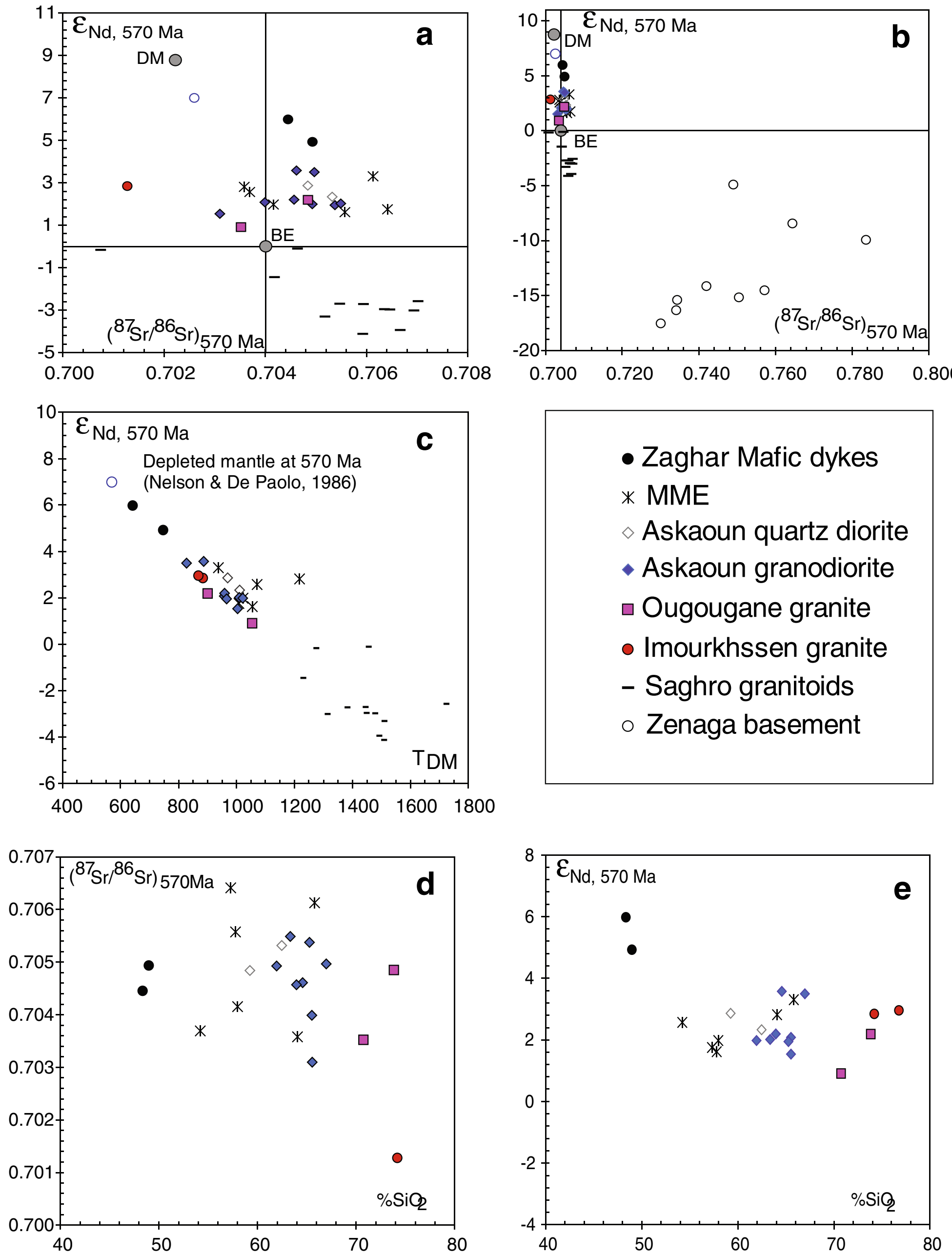

Fig. 7 **a** and **b** Sr and Nd isotopic initial ratios (ε_{Nd} vs $(^{87}Sr/^{86}Sr)_i$ at 560 Ma for the studied rocks and for some references from the Anti-Atlas Belt (Saghro granitoids from Errami et al. 2009; Zenaga basement from Ennih and Liégeois 2008). **c**: $\varepsilon_{Nd560Ma}$ vs T_{DM} model ages; **d** $(^{87}Sr/^{86}Sr)_{560\ Ma}$ vs %SiO_2; **e** $\varepsilon_{Nd560Ma}$ vs %SiO_2

to the volcanic climax of the Ouarzazate Group whose extrusion occurred between 580 and 545 Ma (Thomas et al. 2004; Gasquet et al. 2005, 2008). The Ouarzazate Group extruded during a transtensional period that led to important subvertical movements at the origin of the highly variable thickness of this volcanic sequence (between 0 and >2500 m). This transtensional period corresponds to the end of the Pan-African post-collisional period (Bonin 2004; Bonin et al. 1994; Bonin et al. 1998; Liégeois et al. 1998; Rosenberg 2004; Oyhantçabal et al. 2007), and evolved toward extension during the Cambrian, marking the beginning of the anorogenic period. The geodynamical context of the Tifnoute Valley granitoids is thus well defined; its alkali-calcic/high-K calc-alkaline geochemistry is indeed typical of the post-collisional period (Liégeois et al. 1998; Duchesne et al. 1998; Miller et al. 1999; Bonin 2007).

Tight relationship between shear zones and post-collisional granitoids are linked to a high heat flow able to generate high-temperature metamorphism and granitoids of crustal or mixed crustal/mantle origin (Liégeois et al. 1998). The main cause invoked is uprise of the asthenospheric mantle either due to slab break off (Liégeois and Black 1987) or to linear delamination along mega-shear zone (Liégeois et al. 1998, 2003; Azzouni-Sekkal et al. 2003;

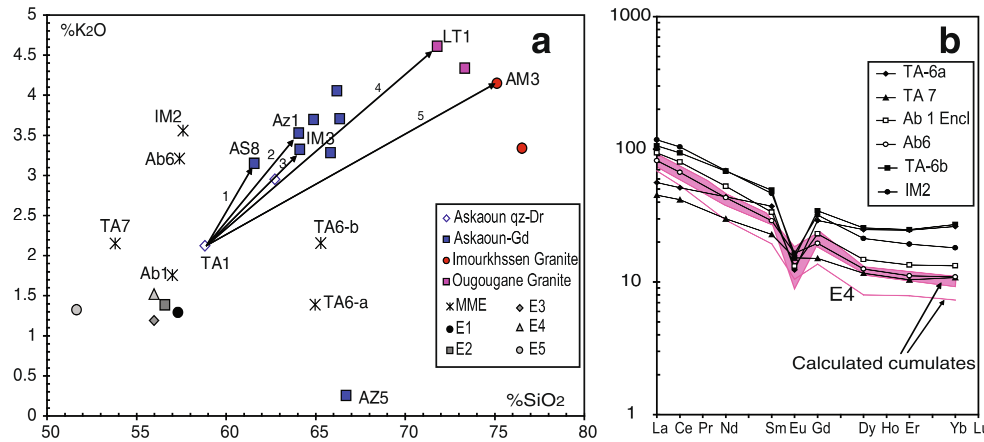

Fig. 8 **a** K_2O vs. SiO_2 diagram illustrating the five modelled evolution and the resulting calculated cumulates (E1 to E5). **b** REE diagram comparing the MME patterns (Ta6a, TA7, Ab1encl, AB6, Ta6b, IM2) and the calculated cumulates, E1, E2, E3 and E5 being represented by the pink area pattern

Acef et al. 2003; Fezaa et al. 2010). This asthenospheric mantle uprising close to the Moho and consequent high regional heat flow can be at the origin of the melting of the lithospheric mantle (Bardintzeff et al. 2010), of the lower crust (Fezaa et al. 2010) but also of the asthenopsheric mantle itself (Hadj-Kaddour et al. 1998). This complex situation is reflected by the telescoping of distinct magmatic suites with various characteristics (Liégeois et al. 1998; Bonin 2004; Seghedi et al. 2004; Williams et al. 2004; Guo et al. 2007) which is often mistakenly attributed to different geotectonic settings (Arculus and Gust 1995; Wilson and Bianchini 1999; Duggen et al. 2005).

A common characteristic of the post-collisional magmatism is that it is generated in a pre-existing lithospheric source, mantle or crust. This lithosphere can be much older or slightly older and bear most often a composition modified by earlier subduction period(s). The partial melting of such sources enhances their characteristics, rendering the produced magmas richer in K_2O and other LILE than those produced during the dehydration of the subducting plate (Liégeois et al. 1998 and references therein). This leads classically to high-K calc-alkaline, partly alkali-calcic, granitoid series. The characteristic Nb-Ta negative anomaly of the subduction-related magmas (Green 1995) is preserved during the remelting of the subduction-related lithosphere (Liégeois et al. 1998; Morrisson et al. 2000) and is an important inherited fingerprint.

In the case of Tifnoute granitoids, we must take into account regional and internal constraints. These are:

(1) Tifnoute granitoids have been precisely dated at 558±2 Ma and 561±3 Ma, demonstrating that they are contemporaneous with the widespread volcanic Ouarzazate Group, covering the whole Anti-Atlas (Fig. 1). This precludes any large horizontal movements between different parts of the Anti-Atlas after their emplacement, including along the AAMF. Constraints extracted from the whole Anti-Atlas must thus be taken into account and the current disposition can be considered as roughly equivalent to the Late Ediacaran disposition. This means that the Ouzellarh Salient in which the Tifnoute granitoids intruded, can be considered as a Late Ediacaran feature, whatever its origin. The South Atlas Fault or the North High Atlas Front (NHAF; Fig. 1) can be considered as Neoproterozoic features. Let us remark that the distinction between the NHAF and the SAF is not needed in Neoproterozoic times, their distinction occurred only during the Mesozoic rifting stage (Laville et al. 2004).

(2) Current Anti-Atlas outcrops result from the uplift of the area as a single entity in consequence of the Cenozoic Europe-Africa convergence (Ruiz et al. 2011). The Variscan orogeny produced severely inverted intracratonic basins all over the belt (Burkhard et al. 2006). Pre-Pan-African Cryogenian lithologies such as the greenschist-facies sediments from the WAC passive margin (c. 800 Ma; Bouougri and Saquaque 2004) or the greenschist facies ophiolites from the Bou Azzer Group (750–660 Ma; Thomas et al. 2004 and references therein) are well preserved and have not been eroded, even during the Pan-African orogeny (630–550 Ma). All these observations points to a common rigid lithosphere corresponding to the northern edge of a fractured but not thickened WAC during the Pan-African orogeny (Ennih and Liégeois 2001, 2003, 2008; Gasquet et al. 2008). This can be considered as a metacratonic behaviour (Abdelsalam et al. 2002; Ennih and Liégeois 2008; Liégeois et al. 2012). Indeed, during the Neoproterozoic Pan-African collision, the Anti-Atlas was in a passive margin configuration. The corresponding active margin was represented by the Peri-Gondwanan terranes that drifted away during the Phanerozoic transtensional regime (Nance et al. 2008 and references therein).

(3) The Ouarzazate Group emplaced within a transtensional tectonic regime. In Bou Azzer-Bleida and Imiter Inliers

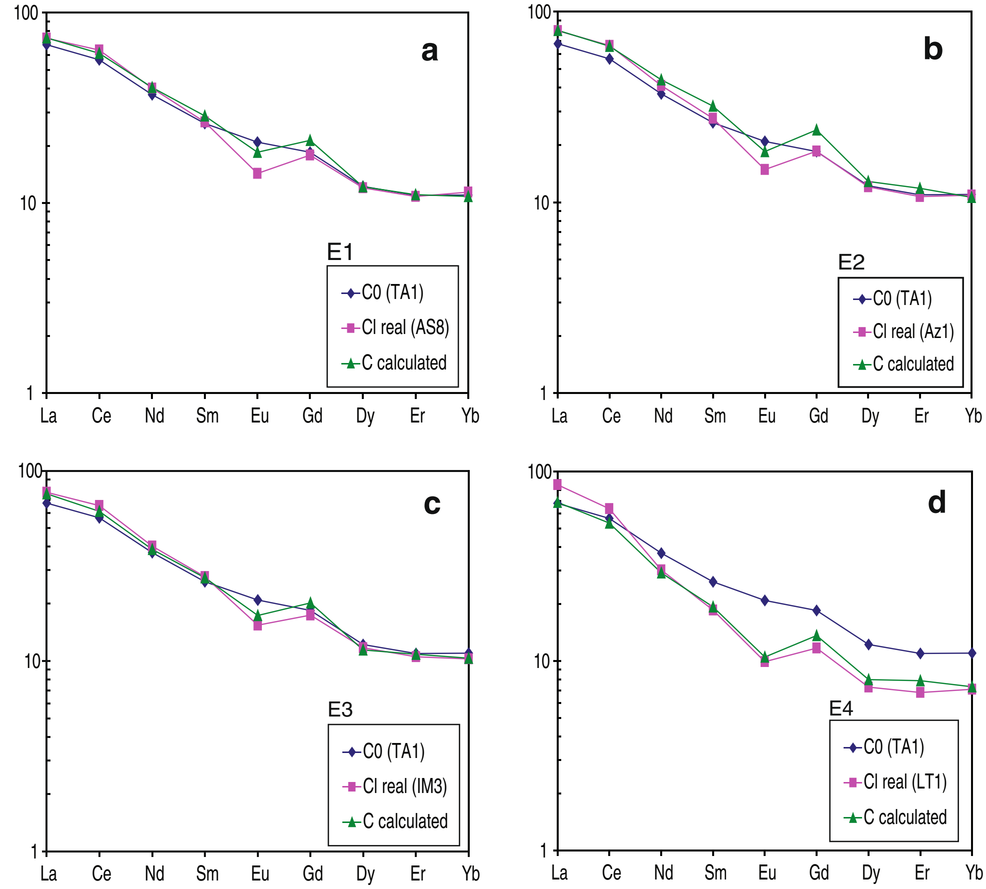

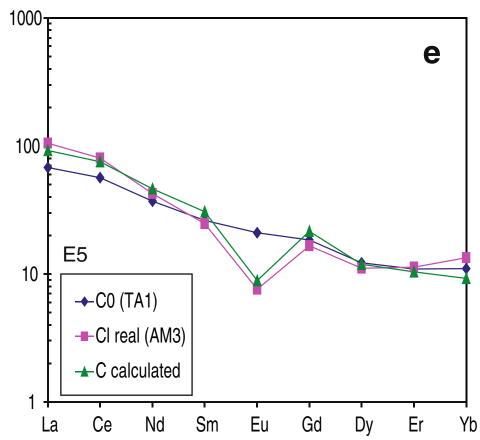

f

KD	La	Ce	Nd	Sm	Eu	Gd	Dy	Er	Yb
Cpx	0.31	0.50	1.20	1.60	1.50	1.90	1.90	1.80	1.60
Opx	0.13	0.15	0.20	0.26	0.17	0.34	0.40	0.65	0.94
Hb	0.31	0.54	1.49	2.43	2.07	2.50	2.60	2.70	2.30
Grt	0.10	2.30	0.70	2.70	1.50	9.0	23	44	38
Ilm	0.005	0.006	0.008	0.010	0.007	0.021	0.028	0.035	0.075
Plg	0.13	0.11	0.070	0.050	1.3 / 4	0.040	0.031	0.026	0.049
Mgn	0.22	0.26	0.30	0.35	0.26	0.28	0.28	0.22	0.18
Bi	0.34	0.33	0.28	0.26	0.24	0.26	3.20	3.70	4.40
K-Fds	0.054	0.043	0.027	0.018	1.130	0.011	0.009	0.008	0.007
All	960	940	750	620	56	440	200	100	54
Ap	25	35	58	64	30	64	58	40	22
Zr	2.00	2.64	2.20	3.14	3.14	12	102	135	527
Mnz	11200	9940	7500	5070	820	5070	3450	1800	200
Sph	46	87	152	204	181	190	206	150	104

Fig. 9 REE patterns resulting from the trace element modelling. A to E represents each time the REE pattern of the initial magma C0, sample TA1, the calculated liquid (C calculated) and the actual liquid (Cl real, with the sample name within bracket). These five modelizations correspond to the five trends of Fig. 8a. **a** TA1 to AS8; **b** TA1 to Az1; **c** TA1 to IM3; **d** TA1 to LT1; **e** TA1 to AM3; **f** Partition coefficient of rare earth elements used

(central and eastern the Anti-Atlas), the Late Neoproterozoic series emplaced during a NNW-SSE extensional event which developed a sinistral transtensional tectonic regime (Azizi Samir et al. 1990; Leistel and Qadrouci 1991; Ouguir et al. 1994; Levresse 2001). The pre-existing discontinuities have controlled the geometry of the normal faults. In the Western part of the Anti-Atlas, the late Neoproterozoic volcanic flows are affected by N170° listric normal faults that correspond to the border faults of kilometric-scale half grabens. These faults are covered by lower Cambrian sediments (Piqué et al. 1999). The magmatic and the structural data in the Agoundis-Ounain and Toubkal area argue for a passive margin rift setting, marked by a North–West facing NE–SW normal faults and by a N30° E fissural system (Pouclet et al. 2007).

(4) The Tifnoute granitoids are alkali-calcic and belong to a high-K calc-alkaline series. Modelling of their geochemical compositions indicates that the various granitoid lithologies are cogenetic and linked by a crystal fractionation. Sr and Nd isotopes exclude an AFC process.

Table 4 Results of the geochemical modelization of major elements by mass balance (PETROMOD software).

N°	Parent rock	Daughter rock	% An	% Plg	% Bi	% Hb	% Cpx	% Ilm	% Magn	% Ap	% FK	% Qz	%All	%Zrc	%Tit	% FC	RSS
Cumulate composition calculated from major elements																	
1	TA1 (60.1 %)	AS8 (62.7 %)	An42	70.0	13.9	0.7	0.0	-	3.6	0.4	-	11.4	*	*	*	53.4	0.0
2	TA1 (60.1 %)	Az1(64.9 %)	An42	66.4	14.2	6.2	0.0	-	2.8	0.2	-	10.2	*	*	*	62.6	0.1
3	TA1 (60.1 %)	IM3 (65.2 %)	An41	69.6	12.7	-	2.9	-	4.8	0.7	-	9.3	*	*	*	58.9	0.3
4	TA1 (60.1 %)	LT1 (72.6 %)	An42	62.7	15.4	8.6	-	-	2.8	0.3	-	10.2	*	*	*	78.6	0.5
5	TA1 (60.1 %)	AM3 (75.7 %)	An45	65.9	12.5	15.9	-	0.1	3.1	0.2	-	2.4	*	*	*	66.9	0.6
Cumulate composition calculated from major elements (recalculated to 100 % without quartz)																	
1	TA1 (60.1 %)	AS8 (62.7 %)	An42	79.0	15.7	0.8	-	-	4.1	0.4	-	*	*	*	*	53.4	
2	TA1 (60.1 %)	Az1(64.9 %)	An42	74.0	15.8	6.9	-	-	3.1	0.3	-	*	*	*	*	62.6	
3	TA1 (60.1 %)	IM3 (65.2 %)	An41	76.7	14.0	-	3.2	-	5.3	0.8	-	*	*	*	*	58.9	
4	TA1 (60.1 %)	LT1 (72.6 %)	An42	69.8	17.2	9.6	-	-	3.1	0.3	-	*	*	*	*	78.6	
5	TA1 (60.1 %)	AM3 (75.7 %)	An45	67.5	12.8	16.2	-	0.1	3.2	0.2	-	*	*	*	*	66.9	
Cumulate composition calculated from REE modelization																	
1	TA1 (60.1 %)	AS8 (62.7 %)	An42	75.9	15.1	0.8	-	3.9	3.9	0.4	-	*	0.05	0.04	-		
2	TA1 (60.1 %)	Az1(64.9 %)	An42	74.0	15.8	6.9	-	-	3.0	0.3	-	*	0.06	0.01	-		
3	TA1 (60.1 %)	IM3 (65.2 %)	An41	76.8	14.0	-	3.2	-	5.3	0.8	-	*	0.05	0.04	0.01		
4	TA1 (60.1 %)	LT1 (72.6 %)	An42	67.7	16.6	9.7	-	-	3.0	3.0	-	*	-	0.20	-		
5	TA1 (60.1 %)	AM3 (75.7 %)	An45	67.5	12.8	16.2	-	-	3.2	0.2	-	*	-	0.08	-		

N° : trend number

-=this mineral is not present

*=not taken into account

Bi : Biotite, Hb : Hornblende; Cpx : Clinopyroxene; Ilm : Ilmenite; Magn : Magnetite; Ap : Apatite; Qz : Quartz. FK : K-feldspar

FC : percentage of fractional crystallization

Number between brackets in column 1 and 2 : SiO_2 wt.%

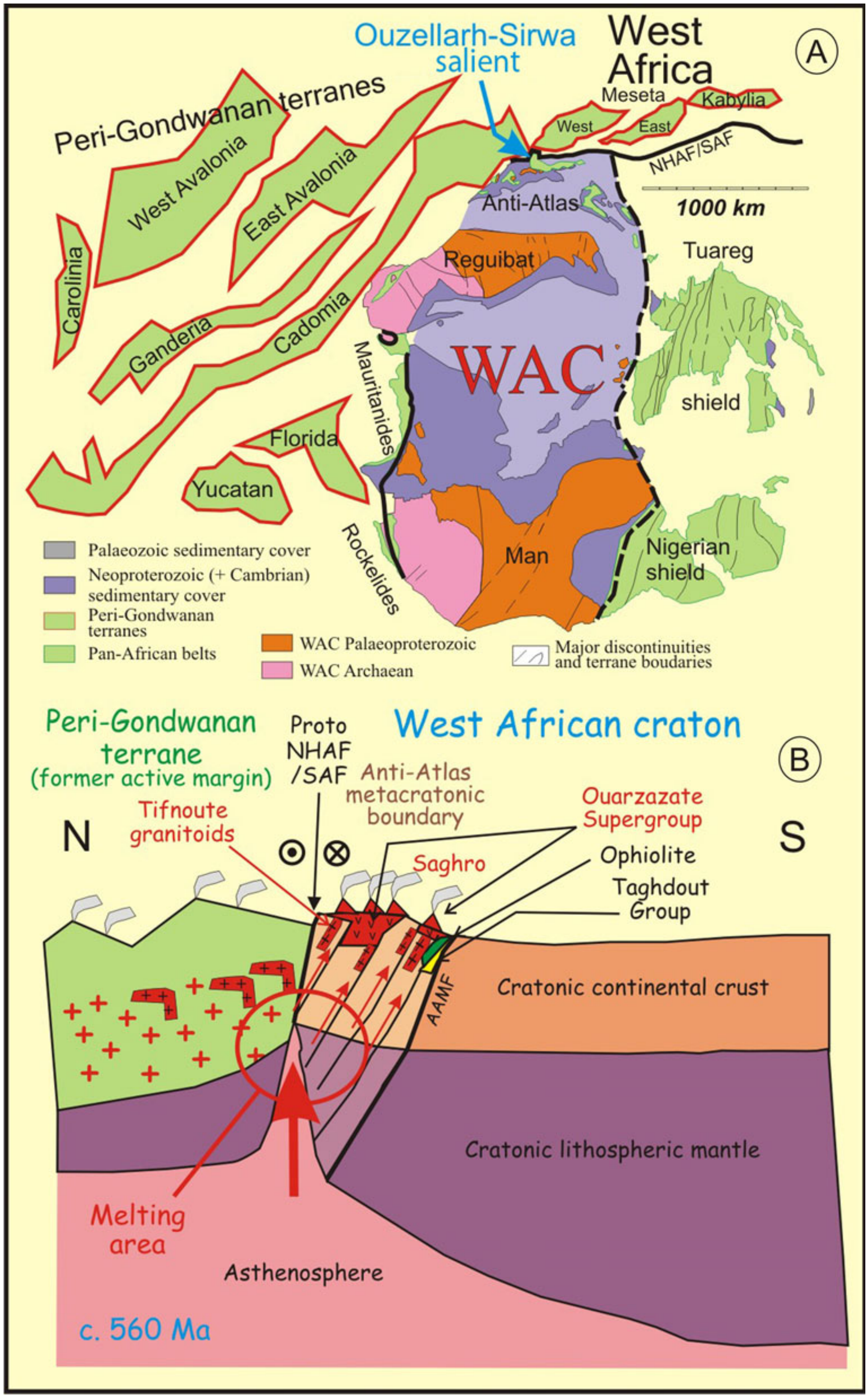

Fig. 10 **a**. Localization of the studied area, the Ouzellarh-Sirwa Salient (OSS), within the West African craton with the representation of the Peri-Gondwanan terranes at c. 560 Ma following Nance et al. 2008 and Ennih and Liégeois 2008. Terranes represented in green belong to the Pan-African belt girdling the West African craton (WAC). Meseta, Kabylia, Tuareg Shield and Nigerian Shield are represented in their present location while the other (Peri-Gondwanan terranes) are located in their postulated position at c. 560 Ma, having moved away since. **b**. Schematic cross-section of the model proposed for the Tifnoute granitoids, at the northern margin of Anti-Atlas, the metacratonic boundary of the WAC (adapted from Liégeois et al. 2012). The latter, fractured but not thickened was invaded by huge amounts of alkali-calcic magmas during Ediacaran but preserved pre-Pan-African lithologies

(5) Sr and Nd isotopes of the Tifnoute granitoids point to a mainly juvenile source (mantle or young lower crust; $\varepsilon_{Nd\text{-}560Ma}$ between +0.8 and +3.5) with some participation of the old basement from the West African craton (NdT_{DM} model ages between 800 and 1200 Ma) in agreement with the few data available in

the area for the Ouarzazate Group (Thomas et al. 2002). This WAC participation is lower than to the east in the Saghro area ($\varepsilon_{Nd\text{-}560Ma}$ between +0.6 and −4 at 560 Ma and NdT_{DM} are between 1000 and 1800 Ma; Errami et al. 2009; Fig. 7).

(6) The late Zaghar mafic dyke swarm has a distinct geochemistry but still has an important Nb-Ta anomaly (Fig. 6l) showing they belong to the same tectonic setting as the Tifnoute granitoids confirming their late Ouarzazate status (Thomas et al. 2002). Their strongly positive $\varepsilon_{Nd\text{-}560Ma}$ (+5 to +6) and young NdT_{DM} model ages (640–750 Ma) indicate that they represent lithospheric mantle partial melts. More samples are needed for a proper characterization of their source.

To explain this regional scale magmatic activity that operated around the NW edge of the West African craton, we propose here a geodynamical model consisting in a post-collisional metacratonic evolution (Liégeois et al. 2012) of the former passive margin (WAC) but close to the terranes of the former active margin (peri-Gondwanan terranes). In other words, we interpret the Tifnoute granitoids and the contemporaneous Ouarzazate Group as the magmatic response, along the plate boundary, of the late Pan-African metacratonic evolution of the northern part of the West African craton, within a transtensive regime.

Linear delamination (Bird 1979; Black and Liégeois 1993) of the WAC continental lithosphere probably began during the climax of the Pan-African convergence marked by transpression (Ennih et al. 2001) but continued during the late Ediacaran transtensional period. The protuberance of the OSS implies the proximity of the subduction-generated lithosphere of the former active margin (peri-Gondwanan terranes). Partial melts of juvenile sources can thus invade the fractured WAC lithosphere, being slightly contaminated by it, and emplaced at shallow level either as subvolcanic plutons (Tifnoute granitoids) or as lava and pyroclastic flows (Ouarzazate Group), during vertical rift-related movements (Fig. 10). This event should have left material in the Anti-Atlas lithosphere that could correspond to the low resistivity anomalies localized in the lower crust recently evidenced by Ledo et al. (2011). These authors suggest that these anomalies could correspond either to relic subducted oceanic sediments linked to the ophiolitic remnants or to the Ouarzazate volcanic group whose emplacement is linked to large fluid movements that have mobilized REE (Ennih and Liégeois 2008) and to worldclass precious metal deposits, base-metal porphyry and SEDEX type occurrence (Gasquet et al. 2005). This study favours the second model, which is also sustained by the postulated presence of the Eburnian basement below the whole Anti-Atlas towards the North High Atlas Front (Ledo et al. 2011).

Other intrusions similar to Tifnoute Valley granitoids are known in the Anti-Atlas, all being alkali-calcic/ferroan granites: Sidi El Houssein (or Tilsakht) pluton in Zenaga (579± 7 Ma), Taourgha pluton in the Bas Draa, Tafraout pluton in Kerdous, Amassine and Imourghane plutons in Siroua. This magmatism evolved to alkaline plutons during the early Cambrian (Jbel Boho alkaline pluton; 529±3 Ma; Gasquet et al. 2005). A similar model can be proposed to the east in Saghro, where the plutons were more contaminated by the Eburnian crust because of their location further from the future SAF/NHAF, the craton boundary.

At the end of the process, the Zaghar strongly mafic dyke swarm could be considered as a crude image of their lithospheric mantle source as for some Malagasy basalts (Bardintzeff et al. 2010). They mark the last stage of the delamination process (Lustrino 2005) just before the Cambrian extension and its alkaline lavas, representing the very last pulses of the asthenospheric mantle.

During the Phanerozoic, the OSS has always played a rigid rheological role, inducing during the Cenozoic the existence of two Cenozoic molassic basins to the south of the High Atlas (Ouarzazate and Souss basins; Fig. 1) and the location of the large Neogene Sirwa stratovolcano (Fig. 1).

Acknowledgments A.T. thanks the Agadir Ibn Zohr University, the Royal Museum for Central Africa and the University of Savoie for financial support (especially the RMCA “Bourses de Stages”) during his PhD. The two anonymous reviewers are greatly acknowledged for their careful review of the paper.

References

Abati J, Aghzer A, Gerdes A, Ennih N (2010) Detrital zircon ages of Neoproterozoic sequences of the Moroccan Anti-Atlas belt. Precambrian Res 181:115–128

Abdelsalam MG, Liégeois JP, Stern RJ (2002) The Saharan metacraton. J Afr Earth Sci 34:119–136

Acef K, Liégeois JP, Ouabadi A, Latouche L (2003) The Anfeg post-collisional Pan-African high-K calc-alkaline batholith (Central Hoggar, Algeria), result of the Latea microcontinent metacratonisation. J Afr Earth Sci 37:295–311

Ahmed AH, Arai S, Abdel-Aziz YM, Ikenne M, Rahimi A (2008) Platinum-group elements distribution and spinel composition in podiform chromitites and associated rocks from the upper mantle section of the Neoproterozoic Bou Azzer ophiolite, Anti-Atlas, Morocco. J Afr Earth Sci 55:92–104

Arboleya ML, Teixell A, Charroud M, Julivert M (2004) A structural transect of the High and Middle Atlas of Morocco. J Afr Earth Sci 39:319–327

Arculus RJ, Gust DA (1995) Regional Petrology of the San Francisco Volcanic Field, Arizona, USA. J Petrol 36:827–861

Azizi Samir MR, Ferrandini J, Tane JL (1990) Tectonique et volcanisme tardi-Pan Africains (580–560 M.a.) dans l'Anti-Atlas Central (Maroc): interprétation géodynamique à l'échelle du NW de l'Afrique. J Afr Earth Sci 10:549–563

Azzouni-Sekkal A, Liégeois JP, Bechiri-Benmerzoug F, Belaidi-Zinet S, Bonin B (2003) The "Taourirt" magmatic province, a marker of the closing stages of the Pan-African orogeny in the Tuareg Shield: review of the available data and Sr-Nd isotope evidence. J Afr Earth Sci 37:331–350

Bajja A (1987) Nouvelles données pétrographiques et géochimiques sur les formations volcaniques précambriennes du Jbel Saghro (Anti-Atlas marocain). Basaltes en coussin du PII et volcanites de la série de Ouarzazate PIII. PhD thesis, H.P. University, Nancy, France

Bardintzeff JM, Liégeois JP, Bonin B, Bellon H, Rasamimanana G (2010) Madagascar volcanic provinces linked to the Gondwana break-up: geochemical and isotopic evidences for contrasting mantle sources. Gondwana Res 18:295–314

Bau M (1996) Controls on the fractionation of isovalent trace elements in magmatic and aqueous systems. Evidence from Y/Ho, Zr/Hf and lanthanide tetrad effect. Contrib Mineral Petr 123:323–333

Beraaouz EH, Ikenne M, Mortaji A, Madi A, Lahmam M, Gasquet D (2004) Neoproterozoic granitoids associated with the Bou-Azzer ophiolitic melange (Anti-Atlas, Morocco): evidence of adakitic magmatism in an arc segment at the NW edge of the West-African craton. J Afr Earth Sci 39:285–293

Berrahma M, Delaloye M (1989) Données géochronologiques nouvelles sur le massif volcanique du Siroua (Anti-Atlas, Maroc). J Afr Earth Sci 9:651–656

Bird P (1979) Continental delamination and the Colorado Plateau. J Geophys Res 84:7561–7571

Black R, Liégeois JP (1993) Cratons, mobile belts, alkaline rocks and continental lithospheric mantle: the Pan-African testimony. J Geol Soc London 150:89–98

Bodinier J, Dupuy C, Dostal J (1984) Geochemistry of Precambrian ophiolite from Bou-Azzer, Morocco. Contrib Mineral Petr 87:43–50

Bonin B (2004) Do coeval mafic and felsic magmas in post-collisional to within-plate regimes necessarily imply two contrasting, mantle and crustal, sources? A review. Lithos 78:1–24

Bonin B (2007) A-type granites and related rocks: evolution of a concept, problems and prospects. Lithos 97:1–29

Bonin B, Bardintzeff JM, Giret A (1994) The distribution of felsic rocks within the alkaline igneous centres. In: Schlich R, Giret A (eds) Géologie, géochimie et géophysique des Kerguelen. Mémoire de la Société Géologique de France, nouvelle série 166:9–24

Bonin B, Azzouni-Sekkal A, Bussy F, Ferrag S (1998) Alkali- calcic and alkaline post-orogenic (PO) granite magmatism: petrologic constraints and geodynamic settings. Lithos 45:45–70

Bouougri EH, Saquaque A (2004) Lithostratigraphic framework and correlation of the Neoproterozoic northern West African Craton passive margin sequence (Siroua–Zenaga–Bouazzer Elgraara Inliers, Central Anti-Atlas, Morocco): an integrated approach. J Afr Earth Sci 39:227–238

Burkhard M, Caritg S, Helg U, Robert-Charrue C, Soulaimani A (2006) Tectonics of the Anti-Atlas of Morocco. Comptes Rendus Geoscience 338:11–24

Cheilletz A, Levresse G, Gasquet D, Azizi Samir MR, Zyadi R, Archibald DA (2002) The Imiter epithermal deposit (Morocco): new petrographic, microtectonic and geochronological data. Importance of the Precambrian-Cambrian transition for major precious metals deposits in the Anti-Atlas. Mineralium deposita 37:772–781.

Choubert G (1942) Constitution et puissance de la série primaire de l'Anti-Atlas. CR Acad Sci Paris 215:445–447

Choubert G (1952) Géologie du Maroc. Fascicule 1, 2ème partie. Histoire géologique du domaine de l'Anti-Atlas. Notes Mém Serv Géol Maroc 100:77–194

Choubert G (1957) Carte géologique du Maroc au 1/500 000, feuille Marrakech. Notes et Mémoires du Service Géologique du Maroc, 70

D'Lemos RS, Inglis JD, Samson SD (2006) A newly discovered orogenic event in Morocco: Neoproterozic ages for supposed Eburnean basement of the Bou Azzer inlier, Anti-Atlas Mountains. Precambrian Res 147:65–78

Dhuime B, Bosch D, Bruguier O, Caby R, Pourtales S (2007) Age, provenance and post-deposition metamorphic overprint of detrital zircons from the Nathorst Land group (NE-Greenland)-A LA-ICP-MS and SIMS study. Precambrian Res 155:24–46

Duchesne JC, Berza T, Liégeois JP, Vander Auwera J (1998) Shoshonitic liquid line of descent from diorite to granite: the late Precambrian post-collisional Tismana pluton (South Carpathians, Romania). Lithos 45:281–303

Duggen S, Hoernle K, Van den Bogaard P, Garbe-Schönberg D (2005) Postcollisional transition from subduction—to intraplate-type magmatism in the westernmost Mediterranean: evidence for continental-edge delamination of subcontinental lithosphere. J Petrol 46:1155–1201

El Hadi H, Simancas JF, Martínez-Poyatos D, Azor A, Tahiri A, Montero P, Fanning CM, Bea F, González-Lodeiro F (2010) Structural and geochronological constraints on the evolution of the Bou Azzer Neoproterozoic ophiolite (Anti-Atlas, Morocco). Precambrian Res 182:1–14

Ennih N, Liégeois JP (2001) The Moroccan Anti-Atlas: the West African craton passive margin with limited Pan-African activity. Implications for the northern limit of the craton. Precambrian Res 112:289–302

Ennih N, Liégeois JP (2003) Reply to comments by E.H., Bouougri. Precambrian Res 120:185–189

Ennih N, Liégeois JP (2008) The boundaries of the West African craton, with a special reference to the basement of the Moroccan metacratonic Anti-Atlas belt. In: Ennih N, Liégeois J-P (eds) The Boundaries of the West African Craton. Geol Soc London, Special Publications 297:1–17

Ennih N, Laduron D, Greiling RO, Errami E, de Wall H, Boutaleb M (2001) Superposition de la tectonique éburnéenne et panafricaine dans les granitoïdes de la bordure nord du craton ouest africain (Boutonnière Zenaga: Anti-Atlas central, Maroc). J Afr Earth Sci 32:677–693

Errami E, Bonin B, Laduron D, Lasri L (2009) Petrology and geodynamic significance of the post-collisional Pan-African magmatism in the Eastern Saghro area (Anti-Atlas, Morocco). J Afr Earth Sci 55:105–124

Evensen NH, Hamilton PJ, O'Nions RK (1978) Rare earth abundances in chondrite meteorites. Geochim Cosmochim Ac 42:1199–1212

Fekkak A, Pouclet A, Benharref M (2003) The Middle Neoproterozoic Sidi Flah Group (Anti-Atlas, Morocco): synrift deposition in a Pan-African continent/ocean transition zone. J Afr Earth Sci 37:73–87

Fezaa N, Liégeois JP, Abdallah N, Cherfouh EH, De Waele B, Bruguier O, Ouabadi A (2010) Late Ediacaran geological evolution (575–555 Ma) of the Djanet Terrane, Eastern Hoggar, Algeria, evidence for a Murzukian intracontinental episode. Precambrian Res 180:299–327

Frizon de Lamotte D, Saint Bezar B, Bracène E, Mercier E (2000) The two main steps of the Atlas building and geodynamics of the western Mediterranean. Tectonics 19:740–761

Frost BR, Frost CD (2008) A geochemical classification for feldspathic igneous rocks. J Petrol 49:1955–1969

Gasquet D, Chèvremont P, Baudin T, Chalot-Prat F, Guerrot C, Cocherie A, Roger J, Hassenforder B, Cheilletz A (2004) Polycyclic magmatism in the Tagragra d'Akka and Kerdous–Tafeltast inliers (Western Anti-Atlas, Morocco). J Afr Earth Sci 39:267–275

Gasquet D, Levresse G, Cheilletz A, Azizi-Samir MR, Mouttaqi A (2005) Contribution to a geodynamic reconstruction of the Anti-Atlas (Morocco) during Pan-African times with the emphasis on

inversion tectonics and metallogenic activity at the Precambrian-Cambrian transition. Precambrian Res 140:157–182
Gasquet D, Ennih N, Liégeois JP, Soulaimani A, Michard A (2008) The Pan-African Belt. In: Michard et al. (eds) Continental evolution: the geology of Morocco. Lecture Notes in Earth Sciences, Springer Verlag, Berlin 116:33-64
Green TH (1995) Significance of Nb/Ta as an indicator of geochemical processes in the crust-mantle system. Chem Geol 120:347–359
Guo Z, Wilson M, Liu J (2007) Post-collisional adakites in south Tibet: products of partial melting of subduction-modified lower crust. Lithos 96:205–224
Hadj-Kaddour Z, Liégeois JP, Demaiffe D, Caby R (1998) The alkaline-peralkaline granitic post-collisional Tin Zebane dyke swarm (Pan-African Tuareg shield, Algeria): prevalent mantle signature and late agpaitic differentiation. Lithos 45:223–243
Hefferan K, Admou H, Hilal R, Karson JA, Saquaque A, Juteau T, Bohn M, Samson S, Kornprobst J (2002) Proterozoic blueschist-bearing mélange in the Anti-Atlas Mountains, Morocco. Precambrian Res 118:179–194
Horstwood MSA, Foster GL, Parrish RR, Noble SR, Nowell GR (2003) Common-Pb corrected in situ U-Pb accessory mineral geochronology by LA-MC-ICPMS. J Ana Atom Spectrom 18:837–846
Ikenne M, Madi A, Gasquet D, Cheilletz A, Hilal R, Mortaji A, Mhaili E (2005) Petrogenetic significance of podiform chromitite from the Neoproterozoic ophiolitic complex of Bou Azzer – Anti-Atlas Morocc. Africa Geosciences Review 13:131–148
Ikenne M, Ennaciri A, Ouguir H, Cousens B, Ziyadi R, Mouhagir M, El-Gaouzi A (2007) Geochemical signature and geodynamic significance of an Ag-Hg mineralized dyke swarm in the neoproterozoic inlier of Imiter – Anti-Atlas (Morocco). Ofioliti 32:109–118
Inglis JD, MacLean JS, Samson SD, D'Lemos RS, Admou H, Hefferan K (2004) A precise U-Pb zircon age for the Bleida granodiorite, Anti-Atlas, Morocco: implications for the timing of deformation and terrane assembly in the eastern Anti-Atlas. J Afr Earth Sci 39:277–283
Inglis JD, D'Lemos RS, Samson SD, Admou H (2005) Geochronological Constraints on Late Precambrian intrusion, metamorphism, and tectonism in the Anti-Atlas Mountains. J Geol 113:439–450
Laville E, Piqué A, Amrhar M, Charroud M (2004) A restatement of the Mesozoic Atlasic Rifting (Morocco). J Afr Earth Sci 38:145–153
Leblanc M (1976) Proterozoic Oceanic-Crust at Bou Azzer. Nature 261:34–35
Leblanc M, Lancelot J-R (1980) Interprétation géodynamique du domaine panafricain (Précambrien terminal) dans l'Anti-Atlas (Maroc) à partir de données géologiques et géochronologiques. Can J Earth Sci 17:142–155
Ledo J, Jones AG, Siniscalchi A, Campanyà J, Kiyan D, Romano G, Rouai M, TopoMed MT Team (2011) Electrical signature of modern and ancient tectonic processes in the crust of the Atlas mountains of Morocco. Phys Earth Planet Int 185:82–88
Leistel JM, Qadrouci A (1991) Le gisement argentifère d'Imiter (Protérozoïque supérieur de l'Anti-Atlas, Maroc). Contrôles des minéralisations, hypothèses génétiques et perspectives pour l'exploration. Chronique de la Recherche Minière 502: 5–22
Levresse G (2001) Contribution à l'établissement d'un modèle génétique des gisements d'Imiter (Ag-Hg) Bou Madine (Pb-Zn-Cu-Au) et Bou Azzer (Co-Ni-As-Au-Ag) dans l'Anti-Atlas marocain. PhD thesis, INPL, Nancy, France
Liégeois JP, Black R (1987) Alkaline magmatism subsequent to collision in the Pan-African belt of the Adrar des Iforas (Mali). In: Fitton JG, Upton BJG (eds) Alkaline Igneous Rocks Geol Soc London, Special Publication 30:381–401
Liégeois JP, Navez J, Hertogen J, Black R (1998) Contrasting origin of post-collisional high-K calc-alkaline and shoshonitic versus alkaline and peralkaline granitoids. Lithos 45:1–28
Liégeois JP, Latouche L, Boughrara M, Navez J, Guiraud M (2003) The LATEA metacraton (Central Hoggar, Tuareg Shield, Algeria): behaviour of an old passive margin during the Pan-African orogeny. J Afr Earth Sci 37:161–190
Liégeois JP, Benhallou A, Azzouni-Sekkal A, Yahiaoui R, Bonin B (2005) The Hoggar swell and volcanism: Reactivation of the Precambrian Tuareg shield during Alpine convergence and West African Cenozoic volcanism. In: Foulger GR, Natland JH, Presnall DC, Anderson DL (eds) Plates, Plumes and Paradigms. Geol Soc Am Special Paper 388:379–400
Liégeois JP, Fekkak A, Bruguier O, Errami E, Ennih N (2006) The Lower Ediacaran (630-610 Ma) Saghro Group: an orogenic transpressive basin development during the early metacratonic evolution of the Anti-Atlas (Morocco). IGCP485 4th meeting, Algiers, p. 57
Liégeois JP, Abdelsalam MG, Ennih N, Ouabadi A (2012) Metacraton: nature, genesis and behavior. Gondwana Res 23:220–237
Ludwig KR (2000) Decay constant errors in U–Pb Concordia intercept ages. Chem Geol 166:315–318
Lustrino M (2005) How the delamination and detachment of lower crust can influence basaltic magmatism. Earth Sci Rev 72:21–38
Michard A, Frizon de Lamotte D, Saddiqi O, Chalouan A (2008) An Outline of the Geology of Morocco. In: Michard A et al (eds) Continental evolution: The geology of Morocco. Lecture Notes in Earth Sciences, vol 116. Springer Verlag, Berlin, pp 1–31
Michard A, Ouanaimi H, Hoepffner Ch, Soulaimani A, Baidder L (2010) Comment on Tectonic relationships of Southwest Iberia with the allochthons of Northwest Iberia and the Moroccan Variscides by J.F. Simancas et al. [C. R. Geoscience 341 (2009) 103–113]
Miller C, Schuster R, Klötzli U, Frank W, Purtscheller F (1999) Post-collisional potassic and ultrapotassic magmatism in SW Tibet: Geochemical and Sr-Nd-Pb-O isotopic constraints for mantle source characteristic and petrogenesis. J Petrol 40:1399–1424
Morrisson GA, Larson PB, Hooper PR (2000) 'Subduction Style' magmatism in a non-subduction setting: the Colville Igneous Complex, NE Washington State, USA. J Petrol 41:43–67
Mortaji A, Gasquet D, Ikenne M, Beraaouz EH, Barbey P, Lahmam M, El Aouli EH (2007) Les granitoides tardi-panafricains de l'Anti-Atlas sud-occidental (Maroc): evolution d'un type magnésien à un type ferrifère. Exemple de la boutonnière de Tifnoute. Estudios Geológicos 63:7–25
Nance RD, Murphy JB, Strachan RA, Keppie JD, Gutiérrez-Alonso G, Fernández-Suárez J, Quesada C, Linnemann U, D'lemos R, Pisarevsky SA (2008) Neoproterozoic-early Palaeozoic tectonostratigraphy and palaeogeography of the peri-Gondwanan terranes: Amazonian v. West African connections. Geol Soc London, Special Publications 297:345–383
Neves SP, Bruguier O, Vauchez A, Bosch D, da Silva JMR, Mariano G (2006) Timing of crust formation, deposition of supracrustal sequences and Transamazonian and Brasiliano metamorphism in the East Pernambuco belt (Borborema Province, NE Brazil): implications for Western Gondwana assembly. Precambrian Res 149:197–216
Oudra M, Beraaouz EH, Ikenne M, Gasquet D, Soulaimani A (2005) La tectonique panafricaine du secteur d'Igherm: implication des dômes extensifs tardi-orogéniques (Anti-atlas Occidental, Maroc). Estudios Geológicos 61:177–189
Ouguir H, Macaudière J, Dagallier G, Qadrouci AY, Leistel JM (1994) Cadre structural du gîte Ag-Mg d'Imiter (Anti-Atlas, Maroc), implications métallogénique. Bull Soc Géol Fr 165:233–248
Oyhantçabal P, Siegesmund S, Wemmer K, Frei R, Layer P (2007) Post-collisional transition from calc-alkaline to alkaline

magmatism during transcurrent deformation in the southernmost Dom Feliciano Belt (Braziliano-Pan African, Uruguay). Lithos 98:141–159

Pearce JA (1980) Geochemical evidence of the genesis and eruptive setting of lavas from Tethyan ophiolites. In: Panayiton A (ed) Ophiolites, Proceeding of International Ophiolites Symposium, Cyprus. pp 261–272

Pearce JA, Harris NBW, Tindle AG (1984) Trace element discrimination diagrams for the tectonic interpretation of granitic rocks. J Petrol 25:956–983

Peccerillo R, Taylor SR (1976) Geochemistry of Eocene calcalkaline volcanic rocks from the Kastamonu area, northern Turkey. Contrib Mineral Petr 58:63–81

Piqué A, Bouabdelli M, Soulaimani A, Youbi N, Iliani M (1999) Les conglomérats du PIII (Néoprotérozoïque supérieur) de l'Anti-Atlas (Sud du Maroc): molasses panafricaines, ou marqueurs d'un rifting fini-protérozoïque? Comptes Rendus Académie Sciences, Paris 328:409–414

Pouclet A, Aarab A, Fekkak A, Benharref M (2007) Geodynamic evolution of the northwestern Paleo-Gondwanan margin in the Moroccan Atlas at the Precambrian-Cambrian boundary. Geol Soc Am, Special Paper 423:27–60

Pouclet A, Ouazzani H, Fekkak A (2008) The Cambrian volcano-sedimentary formations of the westernmost High Atlas (Morocco): their place in the geodynamic evolution of the West African Palaeo-Gondwana northern margin. In: Ennih N, Liégeois J-P (eds) The Boundaries of the West African Craton. Geol Soc London Special Publications 297:303–327

Regragui M (1997) Les formation volcano-sédimentaire et le magmatisme orogénique et anorogénique du néoprotérozoïque supérieur et terminal d'Askaoun (Siroua Occidental, Anti Atlas Central Maroc) Pétrologie, Géochimie et Typologie des zircons. PhD thesis, Université Cadi Ayyad, Marrakech, Morocco.

Rosenberg CL (2004) Shear zones and magma ascent: a model based on a review of the Tertiary magmatism in the Alps. Tectonics 23:1–21

Ruiz GMH, Sebti S, Negro F, Saddiqi O, Frizon de Lamotte D, Stockli D, Foeken J, Stuart F, Barbarand J, Schaer JP (2011) From central Atlantic continental rift to Neogene uplift – western Anti-Atlas (Morocco). Terra Nova 23:35–41

Samson SD, Inglis JD, D'Lemos RS, Admou H, Blichert-Toft J, Hefferan K (2004) Geochronological, geochemical and Nd-Hf isotopic constraints on the origin of Neoproterozoic plagiogranites in the Tasriwine ophiolite, Anti-Atlas orogen, Morocco. Precambrian Res 135:133–147

Saquaque A, Admou H, Karson S, Hefferan K, Reuber I (1989) Precambrian accretionary tectonics in the Bou-Azzer-El Graara region, Anti-Atlas, Morocco. Geology 17:1107–1110

Seghedi I, Downes H, Vasseli O, Szakacs A, Balogh K, Pécskay Z (2004) Post-collisional tertiary-quaternary mafic alkalic magmatism in the Carpathian-Pannonian region: a review. Tectonophysics 393:43–62

Soulaimani A, Piqué A (2004) The Tasrirt structure (Kerdous inlier, Western Anti-Atlas, Morocco): a Late Pan-African transtensive dome. J Afr Earth Sci 39:247–255

Soulaimani A, Bouabdelli M, Piqué A (2003) L'extension continentale au Néo-Protérozoïque supérieur-Cambrien inférieur dans l'Anti-Atlas (Maroc). Bull Soc Géol Fr 147:83–92

Steiger RH, Jäeger E (1977) Subcommission on geochronology: convention on the use of decay constants in geo- and cosmo-chronology. Earth Planet Sc Lett 36:359–362

Thomas RJ, Chevallier LP, Gresse PG, Harmer RE, Eglington BM, Armstrong RA, De Beer CH, Martini JEJ, De Kock GS, Macey PH, Ingram BA (2002) Precambrian evolution of the Sirwa Window, Anti-Atlas Orogen, Morocco. Precambrian Res 118:1–57

Thomas RJ, Fekkak A, Ennih N, Errami E, Loughlin SC, Gresse PG, Chevallier LP, Liégeois JP (2004) A new lithostratigraphic framwork for the Anti-Atlas Orogen, Morocco. J Afr Earth Sci 39:217–226

Veksler IV, Dorfman AM, Kamenetsky M, Dulski P, Dingwell DB (2005) Partitioning of lanthanides and Y between immiscible silicate and fluoride melts, fluorite and cryolite and the origin of the lanthanide tetrad effect in igneous rocks. Geochim Cosmochim Acta 69:2847–2860

Walsh GJ, Aleinikoff JN, Benziane F, Yazidi A, Armstrong TR (2002) U–Pb zircon geochronology of the Paleoproterozoic Tagragra de Tata inlier and its Neoproterzoic cover, western Anti-Atlas, Morocco. Precambrian Res 117:1–20

Wiedenbeck M, Alle P, Corfu F, Griffin WL, Meier M, Oberli F, von Quadt A, Roddick JC, Spiegel W (1995) Three natural zircon standards for U–Th–Pb, Lu–Hf, trace element and REE analyses. Geostandard Newslett 19:1–23

Williams HM, Turner SP, Pearce JA, Kelley SP, Harris NBW (2004) Nature of the source regions for post-collisional, potassic magmatism in Southern and Northern Tibet from geochemical variations and inverse trace element modeling. J Petrol 45:555–607

Wilson M, Bianchini G (1999) Teritiary-Quaternary magmatism within the Mediterranean and surrounding regions. In: Durand B, Jolivet L, Horvàth F, Séranne M (eds) The Mediterranean Basin: Tertiary Extension within the Alpine Orogen. Geol Soc London, Special Publication 156:141–168

Zahour G, El-Khanchaoui T, Chabane A, Youbi N, El-Boukhari A (1999) Les ignimbrites asssociées aux volcanites Néoprotérozoïque du terminal de la boutonnière de Siroua (Anti-Atlas central, Maroc): relation génétique et environnement géotectonique. Africa Geoscience Review 6:177–198